UNIVERSITY OF CALIFORNIA, SAN DIEGO

Investigating the Potential to Control the Morphology of Hydroxyapatite via Micrometer Scale Molding and Casting Techniques

A Thesis Submitted in Partial Fulfillment

Of the Requirements for the Degree of Masters of Science

in

Engineering Sciences (Mechanical Engineering)

by

Ryan Johnson

Committee in Charge:

Professor Olivia A. Graeve, Chair
Professor Shengqiang Cai
Professor Javier Garay

2018

The Thesis of Ryan Johnson is approved, and is acceptable in quality and form for publication on microfilm and electronically:

Chair

University of California, San Diego

2018

Dedication

To my parents who have supported me through all of my years in undergraduate and now graduate studies. I could not have made it this far without you.

Table of Contents

List of Figures

Acknowledgements

This project was funded supported by grant 1334160 from the National Science Foundation. The materials processing was performed in part at the San Diego Nanotechnology Infrastructure (SDNI) of UC San Diego, a member of the National Nanotechnology Coordinated Infrastructure, which is supported by the National Science Foundation (Grant ECCS-1542148). We are grateful for the support of X. Lu for his help in improving the fabrication steps of the process, L. Grissom for help in creating the etching step, and M. Pelella for useful discussions regarding the process as a whole.

ABSTRACT OF THE THESIS

Investigating the Potential to Control the Morphology of Hydroxyapatite via Micrometer Scale Molding and Casting Techniques

by

Ryan Johnson

Masters of Science in Engineering Sciences (Mechanical Engineering)

University of California, San Diego, 2018

Professor Olivia A. Graeve, Chair

Hydroxyapatite (HAp) is an essential biomedical material. HAp's shaping is an important topic in the area of implantology and scaffolding. This project took a novel and unique approach in attempting to to control the morphology of materials without varying parameters such as pH levels, types of solvents, pressure and reaction time. Present work studied the feasibility of controlling the morphology of hydroxyapatite (HAp), with micrometer scale molding and casting. Emphasis was placed on HAp cylinders and cubes of micrometer size. First, cylindrically shaped cavities were patterned and etched with photolithography methods and reactive ion etching techniques on

a Si substrate. Cavities were filled with slurry of deionized water, commercially purchased HAp powder, and Darvan 811 dispersant. Samples were successfully sintered at 1250°C. The obtained samples resembled the cylindrical cavities they were caste in. Scanning electron microscopy (SEM) was used to characterize the size and shape of sintered samples. This technique demonstrates great potential in forming large amounts of homogeneously shaped samples of HAp or similar ceramics for prospective biomedical applications

1. Introduction

1.1 Hydroxyapatite Information

1.1.1 Hydroxyapatite (HAp) background

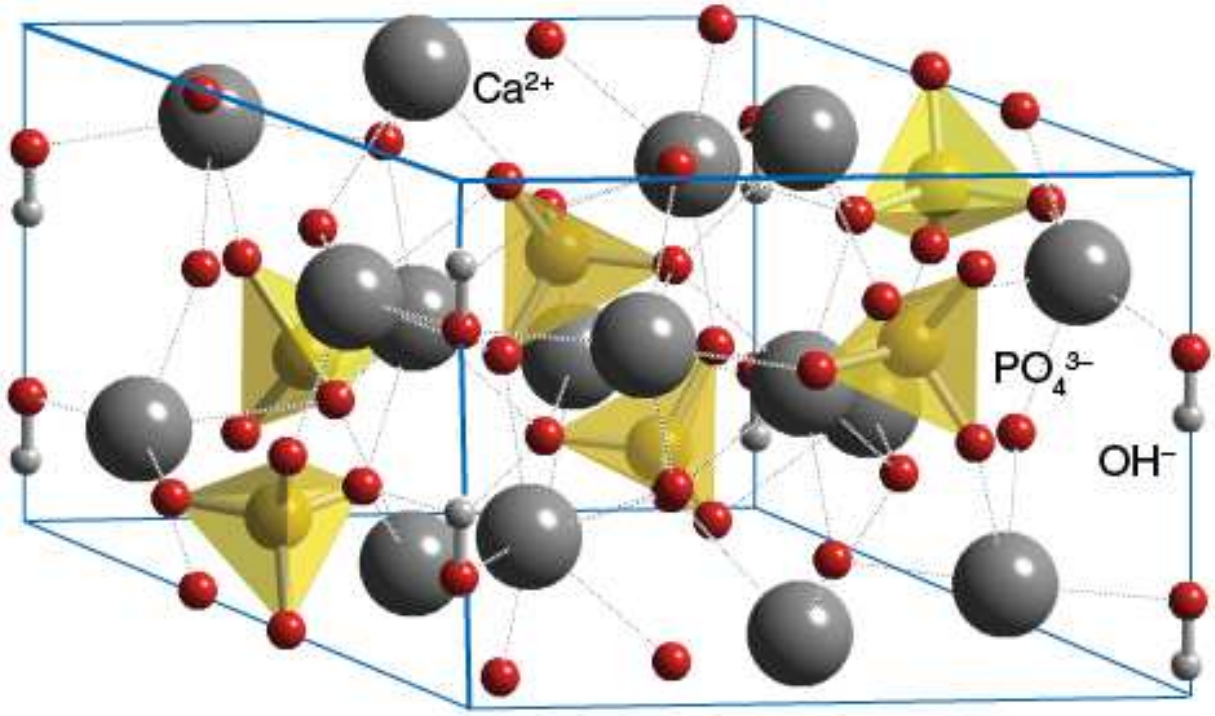

Figure 1 3D representation of a hydroxyapatite molecule [1]**.**

Hydroxyapatite (Ca□□(PO□)□(OH)□, HAp) is a calcium phosphate based ceramic that belongs to the apatite group. Apatite refers to a group of phosphate materials. This group includes hydroxyapatite, fluorapatite and chlorapatite. Members of this family have high concentrations of OH^- , F^- , and Cl^- ions in their crystals which can be easily interchanged between each other to form different apatites. HAp's natural lattice structure is hexagonal dipyramidal. It belongs to the P63/m space group [2]. **Figure 1** is a 3D model of the molecular structure of Hydroxyapatite. It has a stoichiometric Ca/P ratio of 1.67 which is identical to natural bone apatite. HAp is also remarkably stable when it comes to how it behaves in human bodily fluid. When compared to other calcium phosphates, HAp is most stable when placed in pH levels of 4 to 12. It has remarkable

stability when placed in similar temperatures, pH and compositions of human bodily fluids. When added up, these factors lend synthetic HAp to be an invaluable material when working with the human body [3].

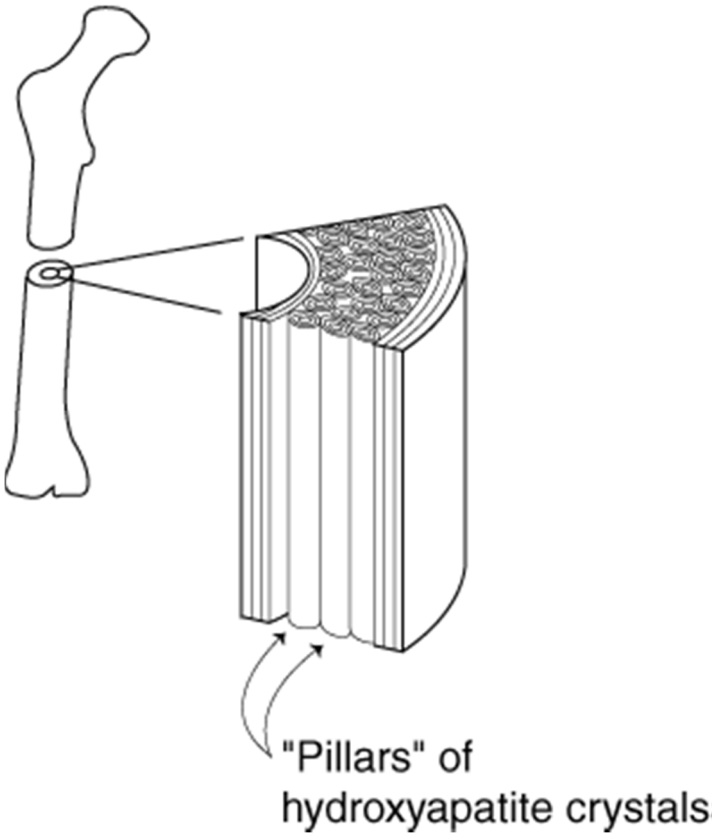

Figure 2 Diagram of the inside of a bone [4].

Human bones are a rigid organ that makes up the vertebrate skeleton of the human body. Bone material is then made up of three major components, collagen, bone minerals and bone matrices. Collagen is the primary structural protein used in the human body, and depending on its mineralization it can be bone, tendons, or cartilage [5]. Bone minerals make up the inorganic portion of the bones and are formed of primarily carbonated hydroxyapatite. Bone matrices are the hardened form of the bone created from layers of osteoblasts that create a honeycomb-like pattern, as seen in **Figure 2**. Osteoblasts are cells that when grouped together can synthesize bone. They

are the cells that combine collagen and bone minerals to form the overarching matrix of bones. Modified HAp makes up to 50% of the volume and 70% of the weight of human bone structures.

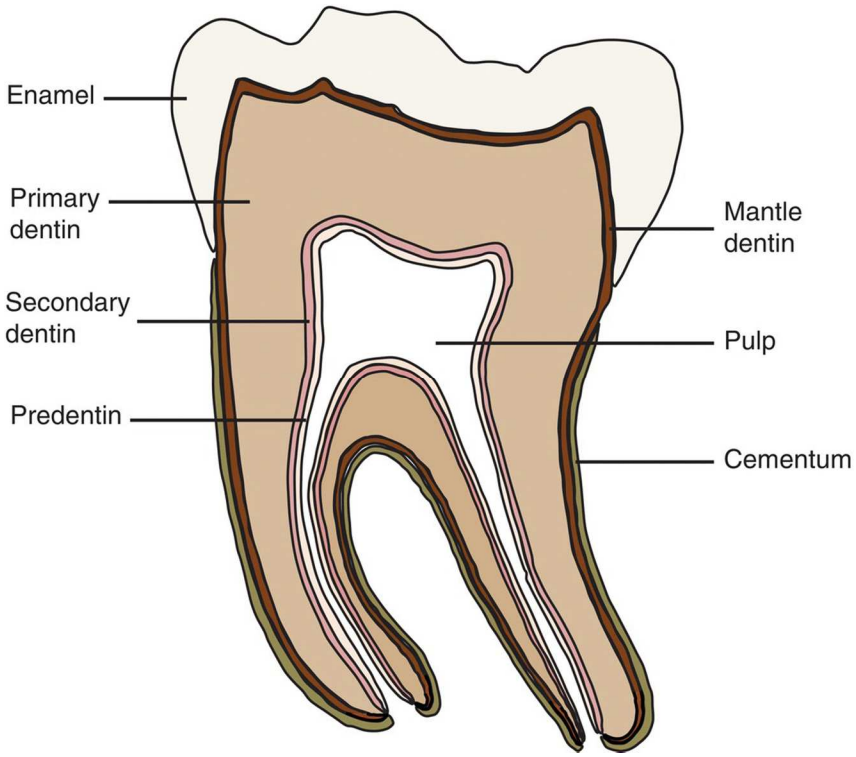

Figure 3 Diagram of the makeup of a human tooth [6].

The main mineral in which teeth enamel and dentin are made up of is another slightly modified form of HAp. The enamel is the hard outer covering of the visible portion of the tooth, or crown, as seen in **Figure 3**. Much like synthetic and natural HAp it is white to off white in color. Dentin is the next layer below the enamel of the tooth. By weight it is 45% HAp, 33% organic material and 22% water. By volume it is 70% inorganic materials, which consists mostly of HAp, 20% organic materials and 10% water [7]. Since the enamel and dentin represents important components of the tooth that ensure the protection of the fragile inner pulp and nerve endings. Finding ways to reinforce these layers and give extra protection is critical to keeping teeth healthy and preventing unnecessary teeth removal.

1.1.2 Uses for HAp and why this is important.

HAp is most commonly found in the biomedical field [8,9,10] where it is used to coat titanium and stainless steel implants [11,12]. It is also seen in enamel repair in toothpaste and mouth-rinsing products [13], and most recently in cheekbone augmentation. In the world of biomaterials there are three categories of materials for use in implants: those that are bioinert, bioactive and biodegradable [14]. Each of these will create different responses from the body. It is important that a material be at least inert, this is because if a material is not bioinert then it can become toxic to the body, which will cause surrounding cells and tissues to die. If a material is nontoxic and bioinert, then fibrous tissue of varying thickness will form, and if it is nontoxic and bioactive then interfacial bonds will form between the material and cells. Originally HAp was a ceramic that excelled in category two, bioactive and biodegradable substances. However, as research has progressed it has shown great promise in use as a bioactive material, specifically in the field of tissue engineering, where HAp is formed into scaffolding structures that stimulate bone growth into them. As a result, HAp's high bioactivity, biocompatibility, osteocompatability, as well as its non-toxic/non inflammatory nature make this an idea material to work within the body.

High bioactivity and biocompatibility are closely related [15]. Bioactivity specifies how well a substance reacts with the body, either negative or positive. Biocompatibility refers to how well a substance is accepted or rejected by the body. In a more broad sense biocompatibility also refers to nontoxicity, noncarcinogenity, chemical inertness and stability in the body. When looking at HAp, its high level for both of these is due to its amazing similarity to natural bone apatite.

Osteocompatability refers to how well an implant in the human body forms bonds with the surrounding tissue. Specifically when osteoblasts attach to the implant and begin to form new bone

structures. A material can have high bioactivity and biocompatibility but it can still have insufficient osteocompatability that then rules it out as a compatible substance for use in the body. Numerous factors can contribute to poor osteocompatability such as inflammation, fibrous capsule formation, and delamination of the surface coatings of implants. These can either prevent osteoblast formations or create weak points in the structures that will collapse in time causing the implant to fail.

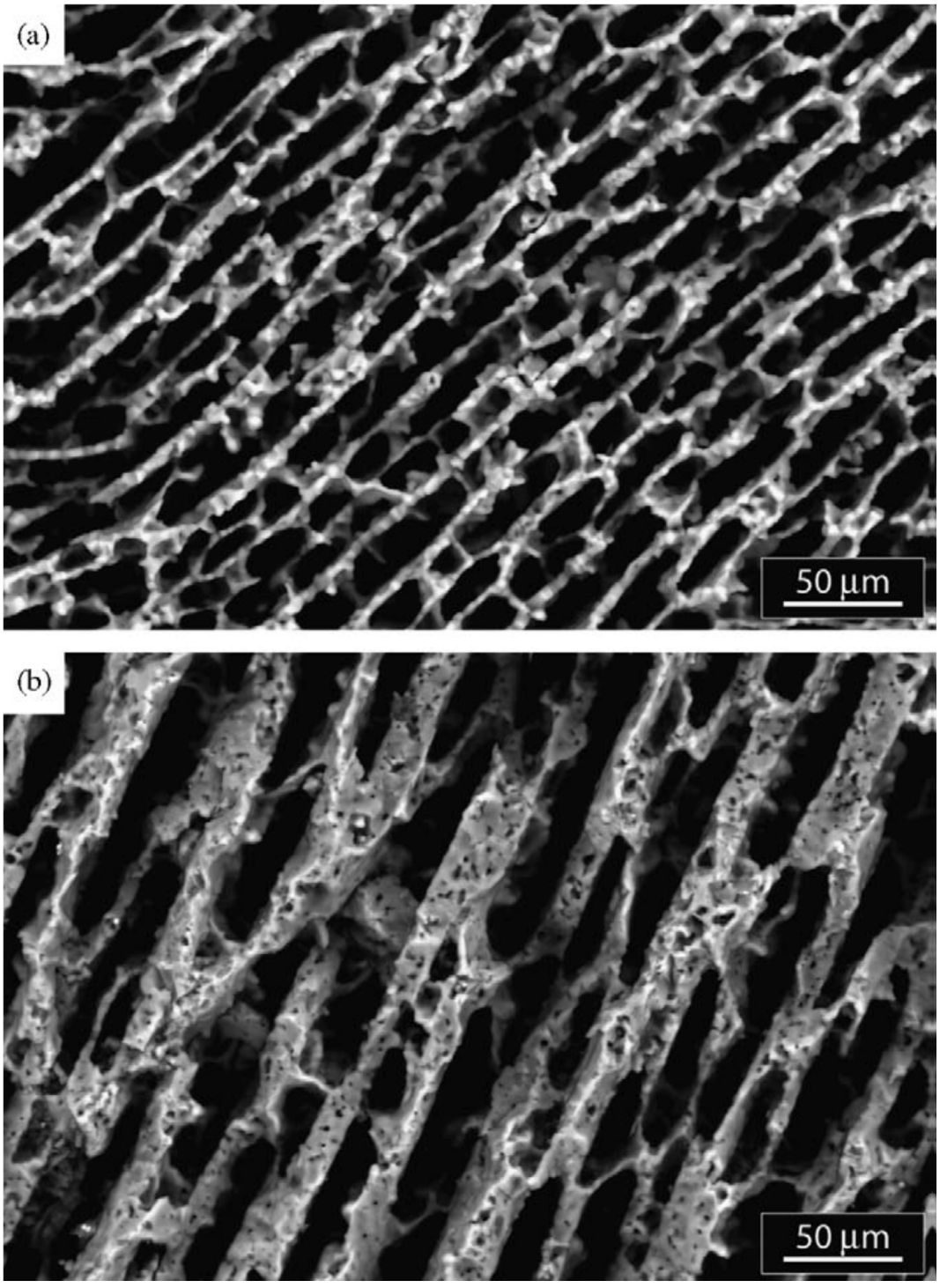

Figure 4 (a) and (b) Freeze casting of hydroxyapatite (reprinted with permission) [19]

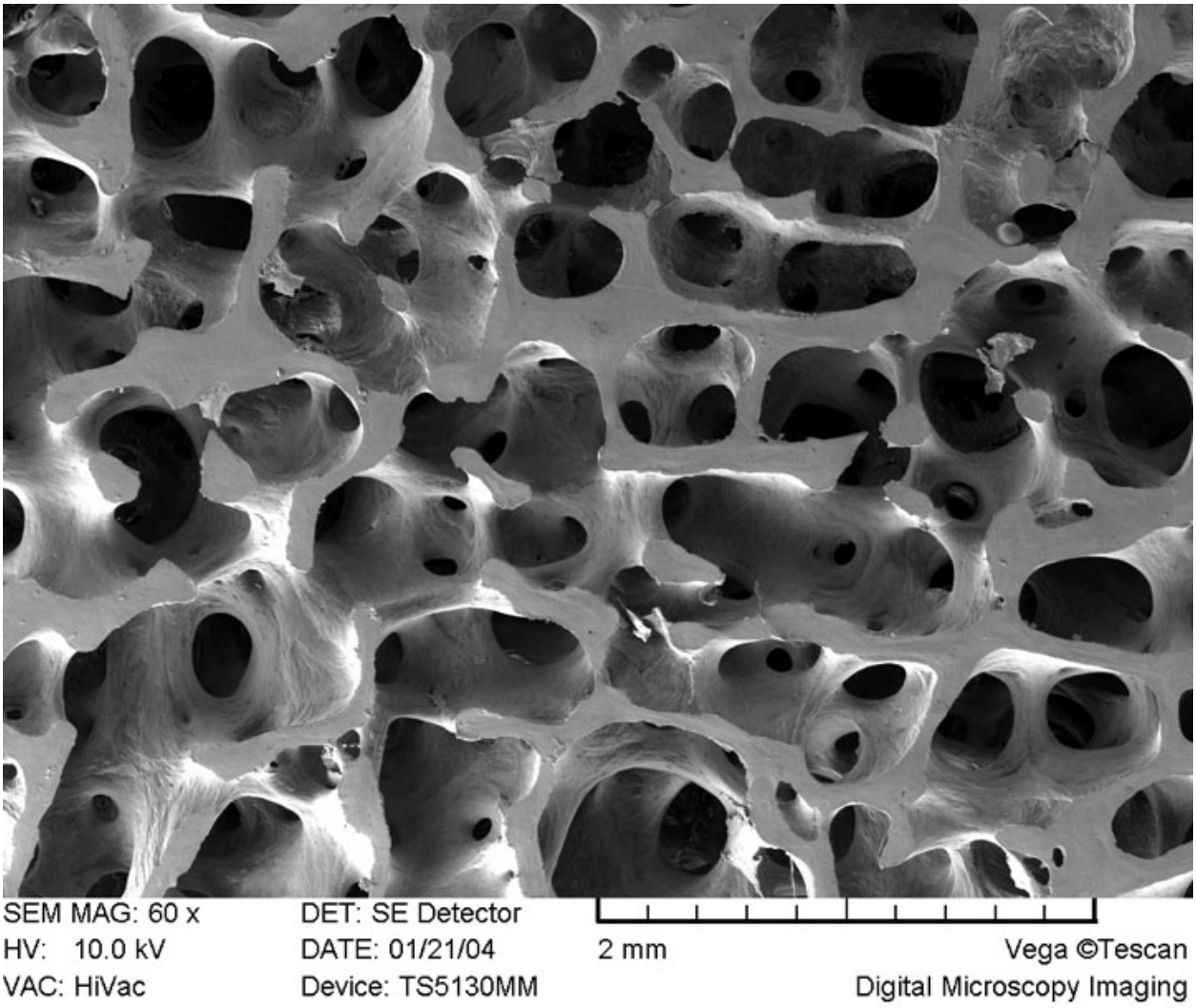

Figure 5 Cross sectional view of a human bone [16].

Currently one of the best ways to facilitate effective osteoblast growth onto implants is to ensure that when implant coatings are sintered, they sinter in a manner that creates porous structures. These porous structures allow osteoblasts to grow more easily into them, and create new bone structures that will fuse natural body tissue to an implant. Current research by other groups is focusing primarily on controlling the shape of the porous structures in order to facilitate a higher load bearing structure. Sintering processes that do not use molds or other additives, such as additional precursors or dispersants, to control the shape end up creating porous structures that

are random in nature and become difficult to describe quantitatively. These random structures tend to be brittle and cannot take high loads. Thus processes have been devised that can better control the shape of the porous structures to help create a more efficient load bearing system. The current most prominent methods are freeze casting, polymer sponge, and 3D printing.

The goal when designing bone scaffolds is to produce complex-shaped scaffolds that have a controlled size, shape, porosity and orientation. The structures produced in **Figure 4** represent another step forward in creating scaffolds that are functionally similar to bone growth. Comparatively **Figures 4**, which is a cross sectional views of porous freeze casted hydroxyapatite, and **Figure 5,** which is a cross sectional view of a human bone are somewhat similar in appearance. Their shapes are somewhat similar, and both have ordered patterns to them, along with proper porosity that will allow fresh bone growth if broken.

Therefore, due to synthetic HAp's biological advantages and similarity to the mineral portion of hard body tissues in the human body. HAp is an ideal material to coat prosthetic implants in order to greatly increase their success rates, as well as filler for amputated bones [17,18]. In particular, the coatings are made of porous scaffolds of HAp which enable fast growth of cells into the structure while being able to handle heavy physiological loads [19,20,21,22].

1.1.3 HAp Synthesis

HAp powder can be produced in bulk by numerous methods [23]. This includes sol-gel [24], solution combustion [25], wet precipitation [26], mechanochemical [27], and hydrothermal techniques [28].

1.1.3.1 Sol-Gel

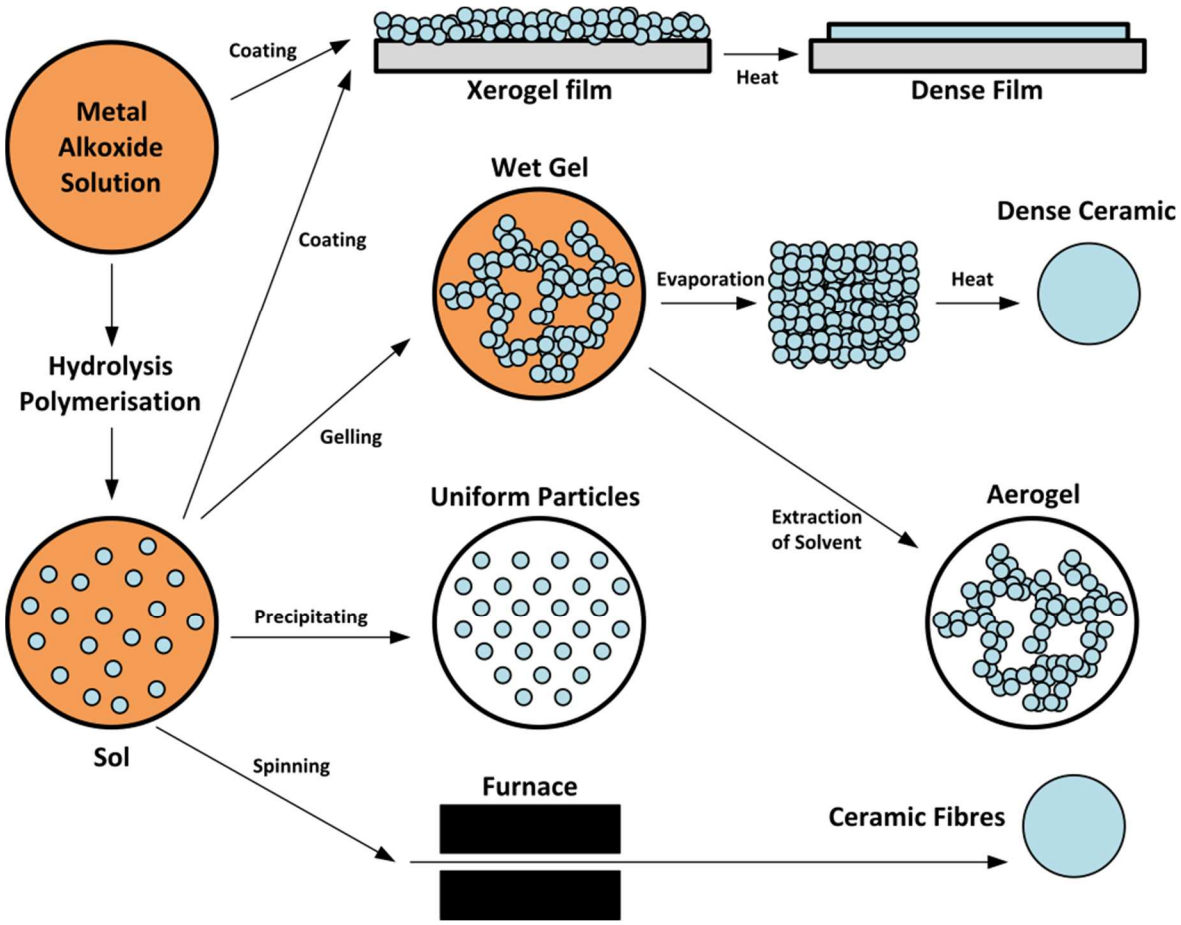

Figure 6 Diagram of sol-gel process [29].

Sol-gel method is a process, which takes a "sol", solution, and changes it over time into a gel-like state. After reaching the liquid/solid phase it can be turned into an aerogel form or, most commonly, a solid ceramic. This method allows high levels of chemical homogeneity and a lower synthesis temperature than needed for other methods such as solution combustion. A major advantage of this process is the ability to achieve densification at much lower temperatures. The material created by the sol-gel process is usually of high purity due to the high control of the temperature allowed for the procedure. Particles created by this method are also nanometer in size, which can improve the reaction and stability at the point of artificial and bone face interaction

[30,31]. There are several disadvantages to the process though. One is the cost of materials can be high. There is also a large amount of shrinkage and cracking that normally occurs during the drying process [32]. The diagram of sol-gel process is shown above in **Figure 6**.

1.1.3.2 Combustion Synthesis

Figure 7 Combustion synthesis reaction

Combustion synthesis is a common method to produce various types of ceramic nanoscale powders [33,34]. Within combustion synthesis are three sub categories of this process: conventional combustion synthesis using solid state reactants, solution-combustion synthesis where the initial reactants are in an aqueous solution, and synthesis of nanoparticles in a flame, or gas-phase combustion. Combustion creates highly pure and homogenous powders and is especially good at creating oxides due to the combustion nature. This synthesis uses salts, such as nitrates, metal sulfates and carbonates, as oxidants, as well as fuels like glycine, sucrose, urea, and other water-soluble carbohydrates.

In general, this method is built on the principle that once the reaction has been started under proper heating conditions, a self-sustaining exothermic reaction occurs for a certain time, which results in a powder as the file product. This rapid exothermic reaction can be seen in **Figure 7**. An advantage of combustion synthesis is the rapid production of fine homogenous powders at a relatively low cost. However, a disadvantage would be the risk of this process because it is an explosion and thus be conducted with care.

1.1.3.3 Mechanochemical

Mechanochemical method is a process where a strong chemical force is applied to materials in order to grind up precursors and create a new substance. This has been done traditionally with a mortar and pestle, as well as ball-milling processes. By having the initial substance come into contact with the ball or pestle, the particle size decreases and the specific surface and surface energy increases. This in turn can promote major structural changes and chemical reactions in the material. A big advantage of this process is that it does not use any solvents, and can be incredibly cheap because the only necessary components are the initial precursors and a ball-milling machine [35,36,37,38].

1.1.3.4 Hydrothermal

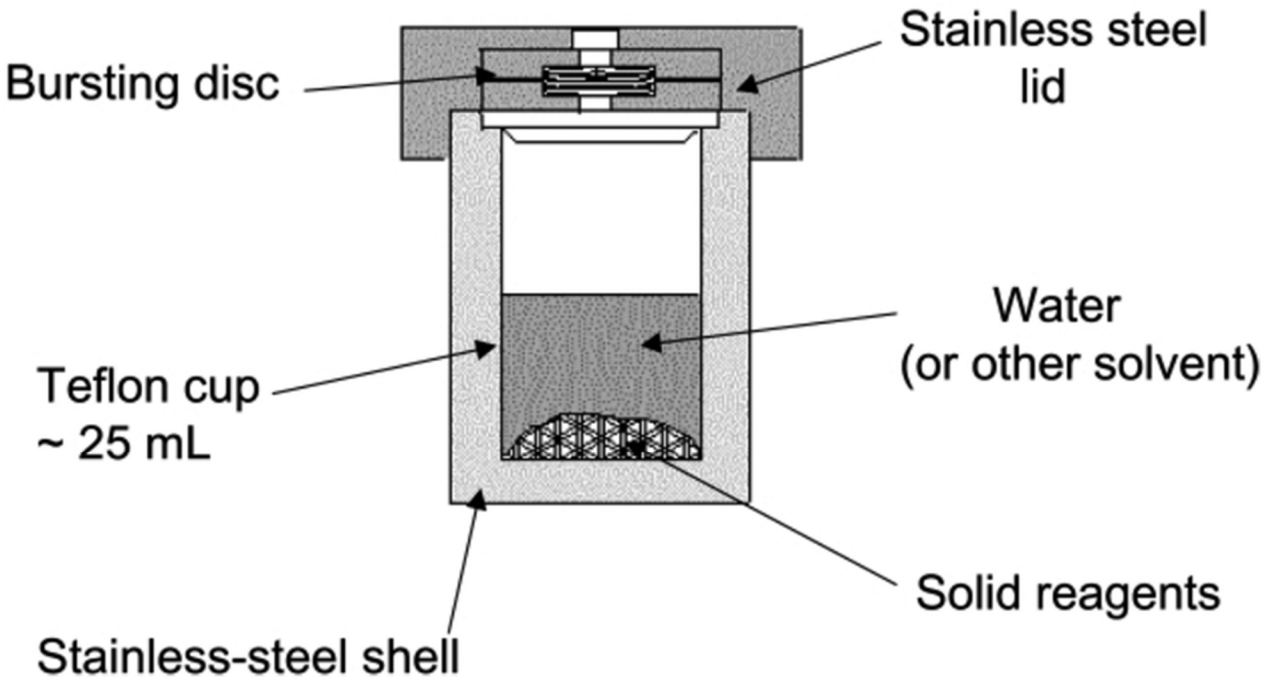

Figure 8 Diagram of an autoclave which is used for hydrothermal synthesis [39].

Hydrothermal synthesis is when aqueous solutions are placed into an autoclave, a pressurized steel cylinder [40]. A diagram of an autoclave used for hydrothermal method is shown in **Figure 8**. The solution is then heated up to high temperatures and pressures for a certain time period. One advantage of this process over others is the ability to grow crystalline phases that are not stable at their melting point. Materials that have high vapor pressure near their melting points can also be grown through this technique. A third advantage is the ability to grow large quantities of quality crystals, while being able to control their composition and growth environments. Disadvantages include the use of extremely expensive autoclaves and the inability to view the growth of the crystals. The diagram of hydrothermal method is shown in **Figure 8**.

1.1.3.5 Wet Precipitation

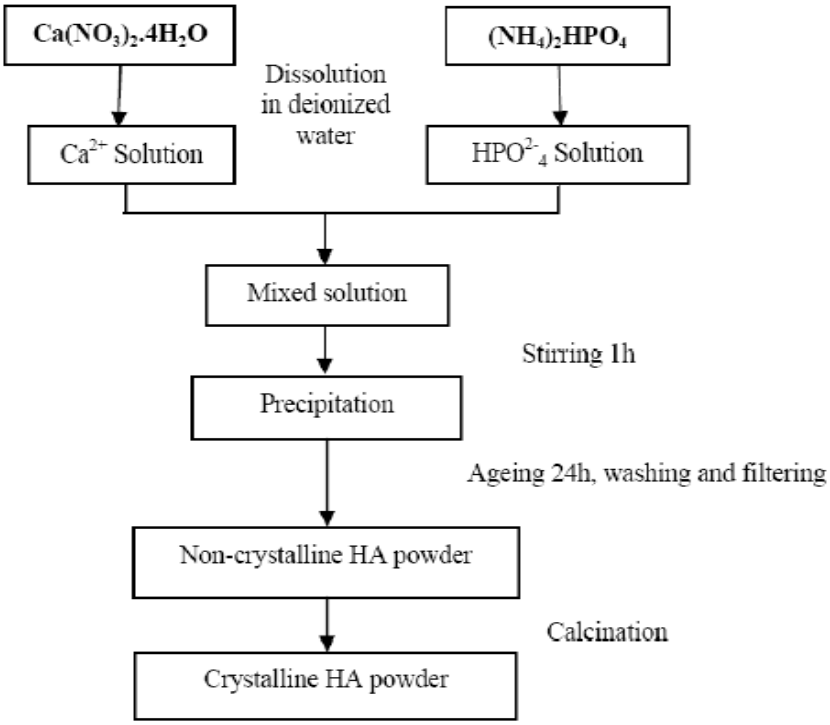

Figure 9 HAp procedure for wet precipitation synthesis (reprinted with permission) [41].

Wet precipitation, also known as chemical precipitation, is the creation of a solid from a liquid solution. **Figure 9** shows the step by step process for wet precipitation method. At least two separate solutions should be prepared, usually consisting of a powder mixed in with water till they are completely dissolved. The initial solutions are then mixed together, sometimes with other precursors, and stirred for lengthy periods of time. Once fully mixed, the solution is dried for a period of time to create a powder, and sintered to produce the final solid sample. One advantage of precipitation method is that it is a proven and simple technique that has been used for many years. Other advantages include good homogeneity, relatively low cost, high purity of product and not requiring any heat treatment. One disadvantage of precipitation is the difficulty to control the

pH over 9 which would results in Ca-deficient HAp. This forms tricalcium phosphates during sintering [42,43,44,45] .

Wet precipitation is the most popular and widely researched of the processes. This is because wet precipitation can create large amounts of powder from a relatively simple process and inexpensive reactants [46,47,48].

1.1.4 HAp Sintering

Sintering is the process of taking a powder and forming it into a solid or porous mass by heating it at high temperatures for a prolonged period of time without melting the material. Several factors must be taken into consideration when sintering: the desired temperature, heating and cooling rates, and holding time. There are also a number of factors, which can influence how the powder sinters, such as particle size, shape, distribution and agglomeration. Sizes and shapes that allow for higher or lower surface area will affect the end density. If distribution and agglomeration of the particles are not well dispersed, then the sintered specimen will result in uneven densification which can limit the strength and hardness of the material.

The most common sintering methods include sintering in conventional furnaces, microwave sintering, plasma sintering, two-step sintering, and hot press sintering.

1.1.4.1 Pressureless Conventional Furnace Sintering

Pressureless sintering is the most common and practical due to its simplicity. This method's main requirement is the use of a high temperature furnace. There are several disadvantages to this process. The largest disadvantage is creation of thermal and residual stress fields that can form on

the surface of samples. This is caused from heating and cooling rates exceeding the heat conductivity of the material. [49,50]

Another downside of this process is the necessity for long heating runs of 10 to 24 hours, or more. This is coupled with holding times of 2 to 4 hours. The importance of these low heating and cooling rates cannot be understated. If a substance it not allowed enough time to heat and cool properly, then thermal cracks can form which can ruin the results [51,52]. Research using this method has sintered specimens of hydroxyapatite using a wide array of temperatures ranging from 800 °C to 1400 °C and heating rates from 20 °C/min down to 0.5 °C/min [53,54,55].

1.1.4.2 Microwave Sintering

Microwave sintering has been studied as a faster alternative method to furnace sintering for different types of ceramic compounds [56]. Instead of applying heat to the outside of the material, microwave radiation heats the substance from within. One advantage of this process is that by heating from within eliminates the likelihood of a thermal gradient forming within the sample that can cause cracking. Microwave's main advantages over traditional furnace heating are that it is a much faster energy conserving process. It conserves energy by using sintering that are incredibly short from 5 to 15 minutes, to the relatively longer times up to 200 minutes [57,58,59].

1.1.4.3 Spark Plasma Sintering

Spark plasma sintering is a technique used to sinter materials at high pressures, low time, and relatively low temperatures (when compared to conventional furnace sintering processes) [60,61,62]. The heating occurs when a pulsed direct current is passed through a conducting die into the material. This causes extremely rapid heating and cooling rates, which limits crystal growth [63,64,65]. Typically plasma sintering is done at a couple hundred degrees but can go well above this up to 1400 °C or more if necessary. Generally this process allows the densification of nano-powders or structures without coarsening.

1.1.4.4 Two-step sintering

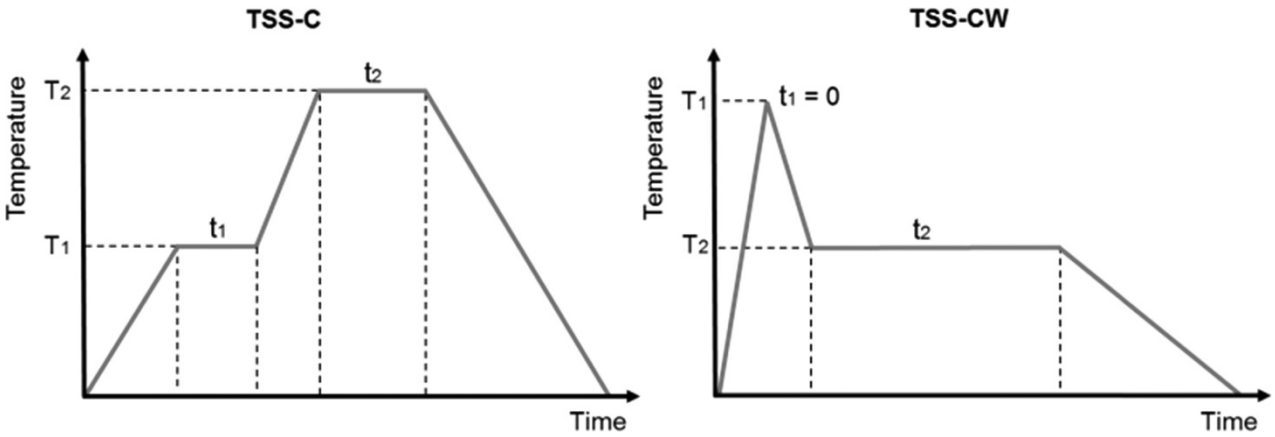

Figure 10 Diagram of the heating and cooling cycle for two step sintering processes: TSS-C and TSS-CW (reprinted with permission) [71].

Two-step sintering (TSS) is a sintering technique that splits the sintering process into two different stages. The initial stage is a pretreatment phase that is performed at relatively low temperature. This is followed by a high-temperature state, and then a cooling phase. The cooling is done rapidly to suppress the grain growth, which occurs during the high temperature stage, but still allow full densification of the material. Within TSS there are two main methodologies, what TSS-C and TSS-CW, TSS-C has an initial low temperature that is held, then sintered at a much

higher temperature, then cooled relatively quickly. TSS-CW starts with a very high heating rate and then rapidly cools to a lower temperature where the material is held for a long period, then cooled. Both are relatively similar, although TSS-CW allows for smaller grain sizes while maintaining the same density measurements as TSS-C. **Figure 10** shows a more detailed diagram of the different heating and cooling rates for the two different types of two-step sintering processes.

Overall this method allows for the formation of dense materials with smaller grain sizes. A great advantage of this process over other sintering methods is its low cost, as well as its high level of control of the microstructure. [66,67,68,69,70,71]

1.1.4.5 Hot Pressing

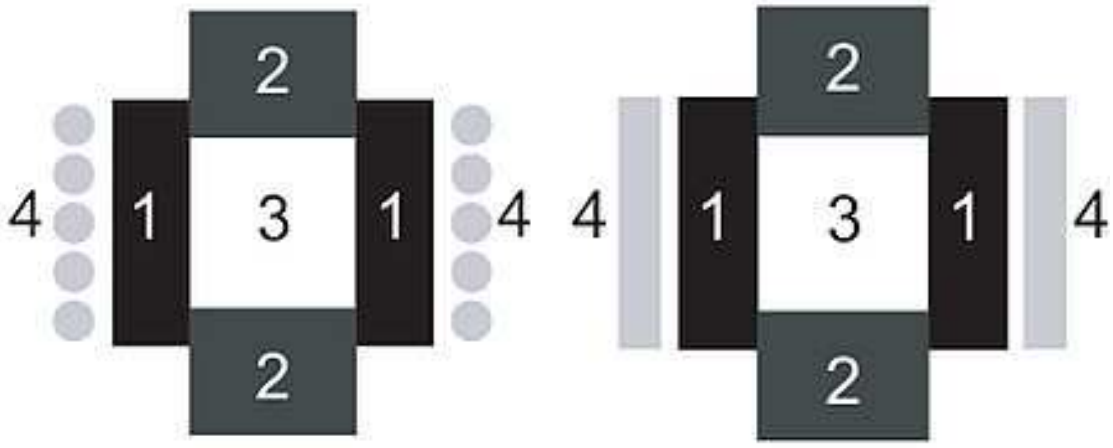

Figure 11 Diagram of different hot pressing setups, (1) mold, (2) pressure applicators, (3) ceramic powder, (4) , (a) inductive heating, (b) indirect heating [72].

Hot pressing is a way to use high pressure and low strain rate to form powders. With high enough pressures and temperatures hot pressing can also be used as a sintering process. This method is used primarily to create hard and brittle substances. **Figure 11** shows a diagram of two different hot pressing types. The loose or compacted powders are poured into graphite molds. These molds are then heated via induction. Indirect resistance heating or field assisted sintering

technique are used to heat the material up to 2400 °C with pressure of up to 50MPa applied if necessary [72,73].

With inductive heating the heat is produced from within the mold using induction coils. One advantage is that pressure and inductive power are independent; the downside is that it is expensive due to the need for a high-frequency generator. Using indirect heating, the mold is placed within a heating chamber and the heat is transferred to the material via convection. Another advantage is the ability to reach very high temperatures. The biggest disadvantage is the large amount of time needed to heat and cool down the mold. In field assisted sintering technique an unpulsed AC or DC current is passed through the material and mold, heating it from within. The method is also known as spark plasma sintering, which was described about earlier. This process results in high heating and cooling rates and reduces the required temperature and pressure needed for sintering. If the current is pulsed, then it is known as direct hot pressing; recent research suggests that there is no huge difference between the two. Thus constant or pulsed currents will produce the same results [74,75,76,77].

1.2 Silicon Substrate

Silicon is the second most common element on the earth and seventh most common element in the universe. It is the most common semi-conductor material and used throughout the technology sector. Silicon is an integral part of integrated circuits, which are key to modern society. A silicon wafer is a thin slice of this semiconducting material, which acts as the substrate to place or grow other electronic devices on top. Due to silicon's ability to absorb photons it is used in both sensors, due to its light sensitivity, and solar cells due to its ability to create electricity.

Silicon substrates serve as substrates for microelectronic devices that are built into and over the wafer. The wafer can undergo many microfabrication steps that include doping, ion implantation, etching, deposition of materials, and photolithography. Once the building of the microcircuits are complete, the wafer is then diced into the proper size. Size of wafers can vary from 1 to 12 inches and thickness that range from 275 μm to 775 μm. However, 4 inch wafers are the most common size.

1.3 Photolithography

Photolithography is a process used in microfabrication work to create patterns on a substrate. Photolithography uses a light sensitive material known as a photoresist to transfer a geometric shape or pattern from a mask onto a substrate. Then through a series of chemical processes the pattern is engraved onto the substrate or deposits a new material onto the pattern. One disadvantage is that the sensitivity of these steps requires the need of processing facilities that are both very clean and have UV sensitive lights. Another disadvantage is that this process requires a flat substrate because using non-flat surfaces is difficult if not impossible to work with.

There are several different lithographic methods: optical lithography (photolithography), electron beam lithography, x-ray lithography and ion beam lithography. Photolithography uses UV light shined through a photomask to imprint a design into a photoresist. Electron beam lithography uses a concentrated ion beam that is scanned across the surface. The advantage of this type is that there is no need for a photomask. This process allows for extremely high levels of precision, down to 10 nm or less if optimized correctly. A disadvantage is that this process is extremely time consuming and expensive.

1.3.1 Photomask

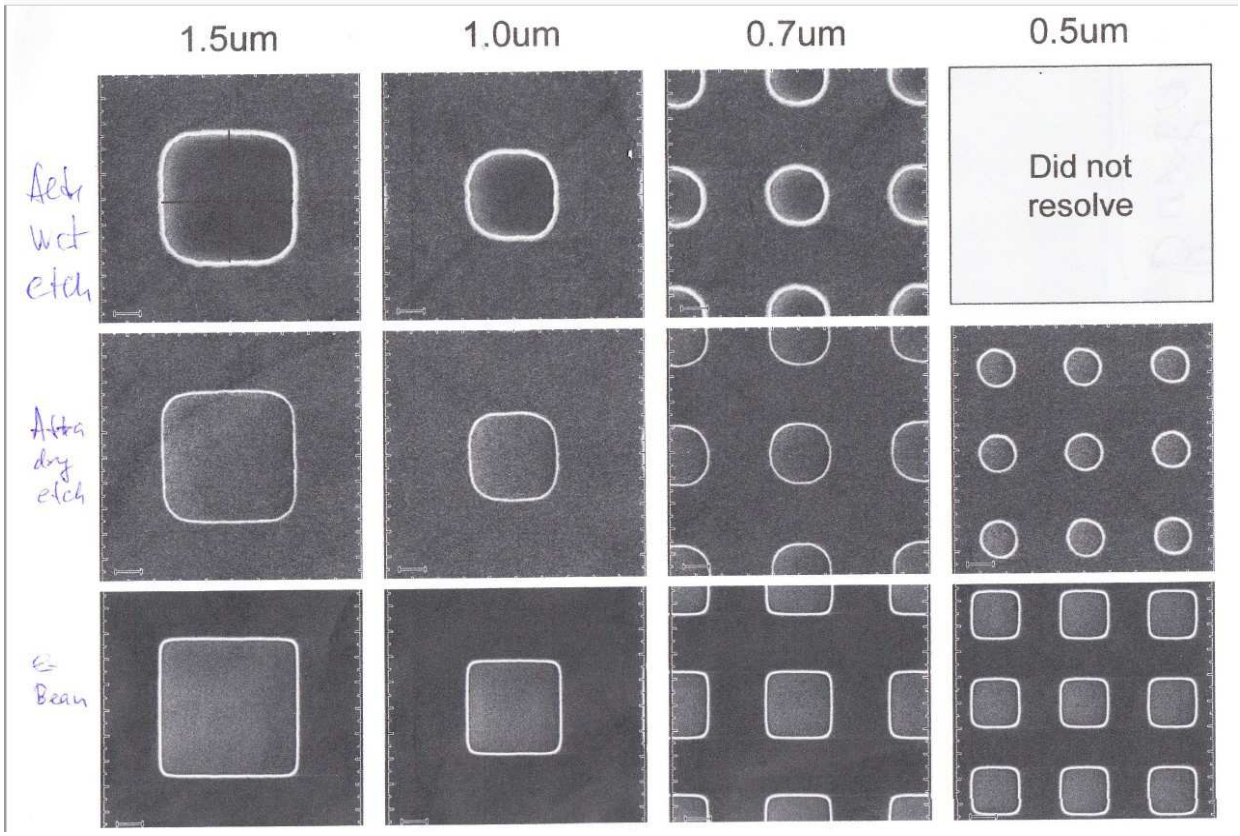

Figure 12 Diagram of different photomask resolutions, produced from top to bottom, wet etching, dry etching and e-beam.

Photomasks are quartz plates of varying sizes, usually 4” x 4” to 9” x 9”, that allow light to shine through them in a predefined pattern. The mask uses silver, chrome, chrome oxide, iron oxide, copper, or other materials to create opaque regions on it. Depending on how the mask is designed, patterns can be created by using these opaque and clear regions.

Masks have varying levels of quality that can determine how long it is used, based on what material it was made of, or the precision of its pattern due to precision of its design. Pricing of photomasks can vary from three hundred dollars to upwards of ten thousand dollars. These prices are based upon the precision and defect size of the given mask. The precision and defect size can range from the nanometer scale to small micrometers depending on what lithography type and

etching process were used. **Figure 12**, demonstrates visually the difference between different resolutions of photomasks. Different sized squares were made with three different methods, wet and dry etching, as well as e-beam lithography. From these squares it is clearly visible how resolutions improve from top to bottom.

1.3.2 Photoresist

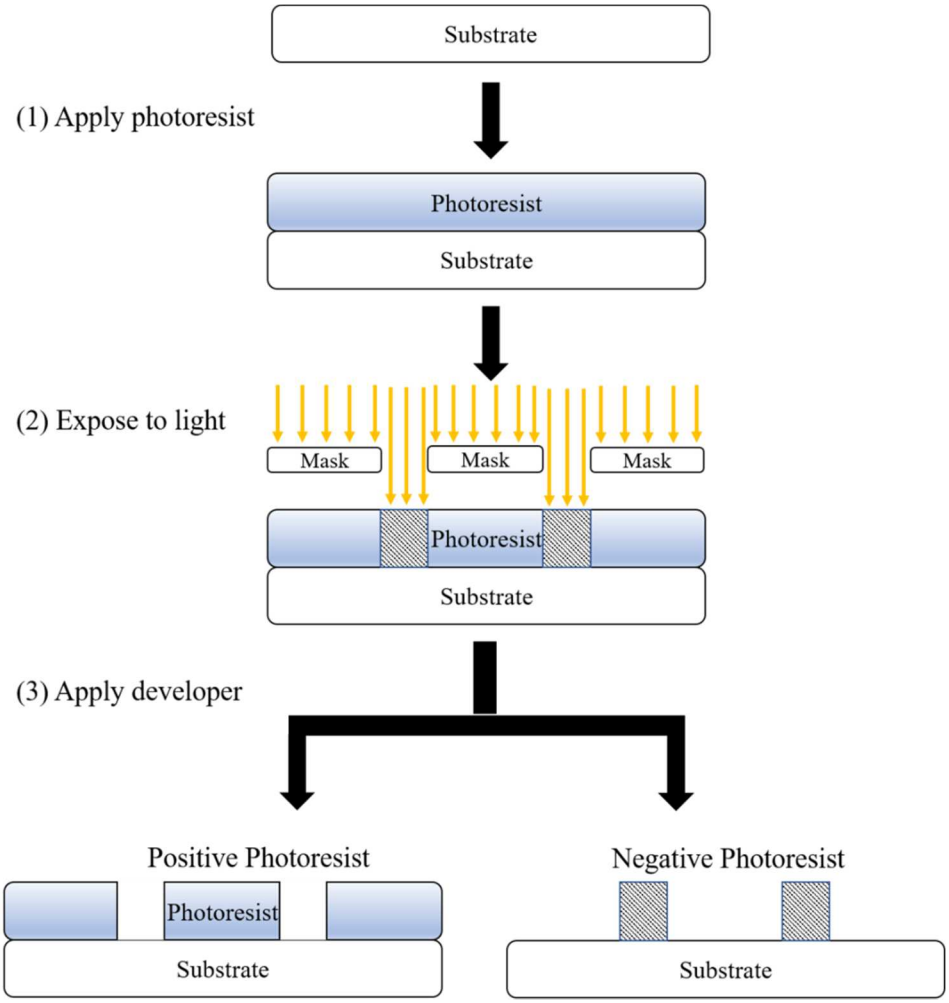

Figure 13 Diagram of photoresist procedure. Beginning with (1) applying photoresist, (2) exposure to light, and (3) apply the developer to either positive or negative resists [78].

Photoresists are a light-sensitive material used in photolithography and photoengraving. In photolithography there are two types of photoresists that are used, positive and negative. Positive resists become soluble when exposed to UV light, unexposed areas stay insoluble. Negative photoresists become insoluble when exposed to UV light, and the unexposed portion can be developed and washed away. There are numerous other differences between the two. The most important are that positive resists are able to gain higher resolution than negative resists. Negative resists tend to also be less expensive than positive ones.

Figure 13 summarizes the main steps of photoresist procedure, including both, positive and negative photoresists. The general procedure of photolithography is to apply the photoresist, **(1)**, expose to UV light, **(2)**, and develop and clean the resist, shown in (**3)**.

1.4 Lift-off process

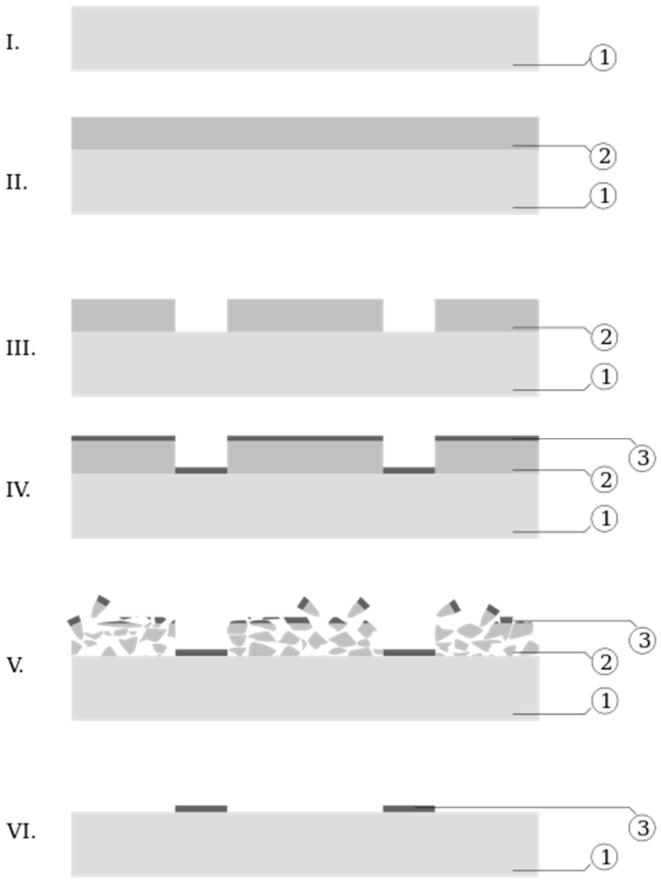

Figure 14 Diagram of lift-off process (i) start with clean substrate (ii) addition of photoresist, (iii) patterning and development of resist, (iv) deposition of metal layer, (v) removal of resist, (vi) cleaning of substrate. (1) substrate (2) photoresist (3) metal layer [78].

Lift-off process is a technique used in microfabrication that employs a sacrificial material to create a structure or pattern on a material. It is an additive technique, where in the end the substrate is left with more than what was started with, unlike etching with subtracts material. Normally, a photoresist is placed on a clean substrate, shown in **Figure 14 (I)** and **(II)**. A pattern

is then exposed onto the resist, shown in **Figure 14 (III)**. After developing the resist, a thin layer of metal is deposited, **Figure 14 (IV)**. The metal will cover what remains of the photoresist as well as the bare areas that were developed and washed away, **Figure 14 (V)**. Finally, the photoresist is washed away leaving only the metal on the substrate, **Figure 14 (VI)**. This method is used to create what is known as a hard mask on top of the substrate. Thus this is usually used when etching of the material would have an undesirable effect on the layer below. There are three main disadvantages to this process. The first disadvantage is retention. This is when parts of the metal remain on the wafer despite the washing. The second one is what is known as "ears can appear". This is when metal is deposited on the sidewalls of the resist. When this occurs earlike formations can form on the edges and show up when the resist is washed away. These metal layers have raised edges instead of being flat, due to being built up against the sidewalls. The third disadvantage is redeposition. This issue is a hard step to control as it occurs during the lift-off process. This is when small particles of metal reattach themselves to the surface after lift-off.

1.5 Etching processes

Etching is the process of removing previously deposited layers and/or the substrate of the sample. Traditionally this is done in one of two ways, wet or dry etching.

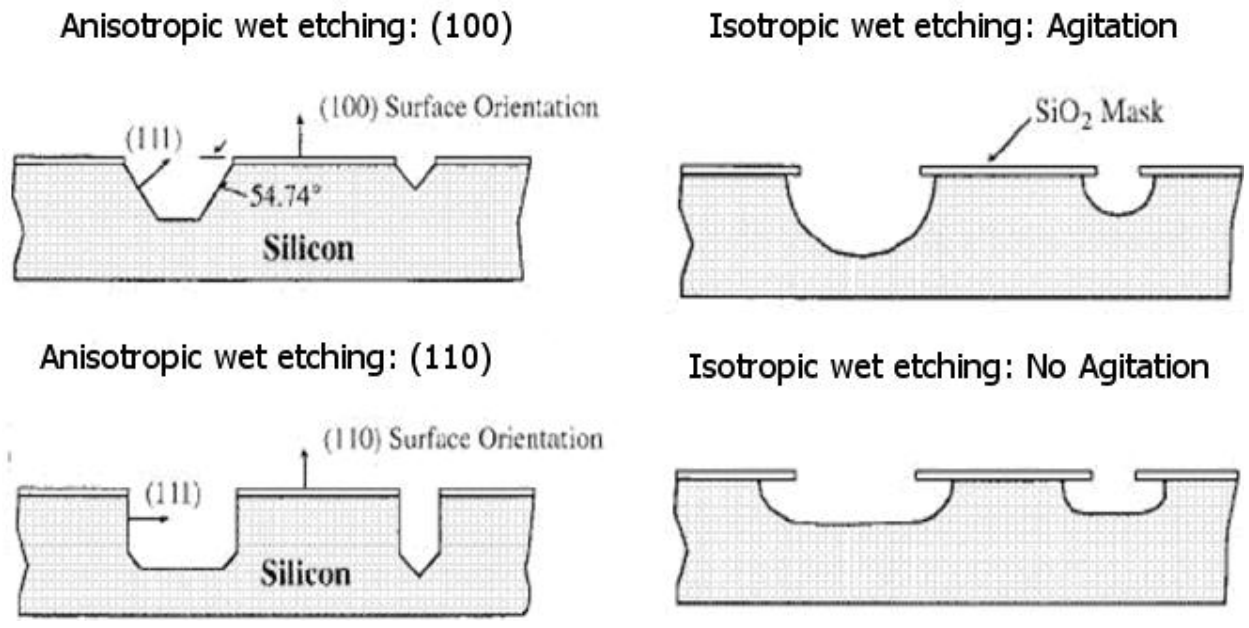

Figure 15 Diagram of the different wet etching types [79].

Wet etching is the simpler of the two and uses a liquid solution that dissolves the sample. The solution itself is either a chemical etchant or a type of acid, most commonly hydrofluoric acid, phosphoric acid, and potassium hydroxide. Most wet etchants will etch isotropically, in all directions. **Figure 15** shows different types of wet etching. This method is most useful when etching surfaces that have small features. The biggest disadvantages are inability to etch small and detailed surface features, and the creation of toxic byproducts.

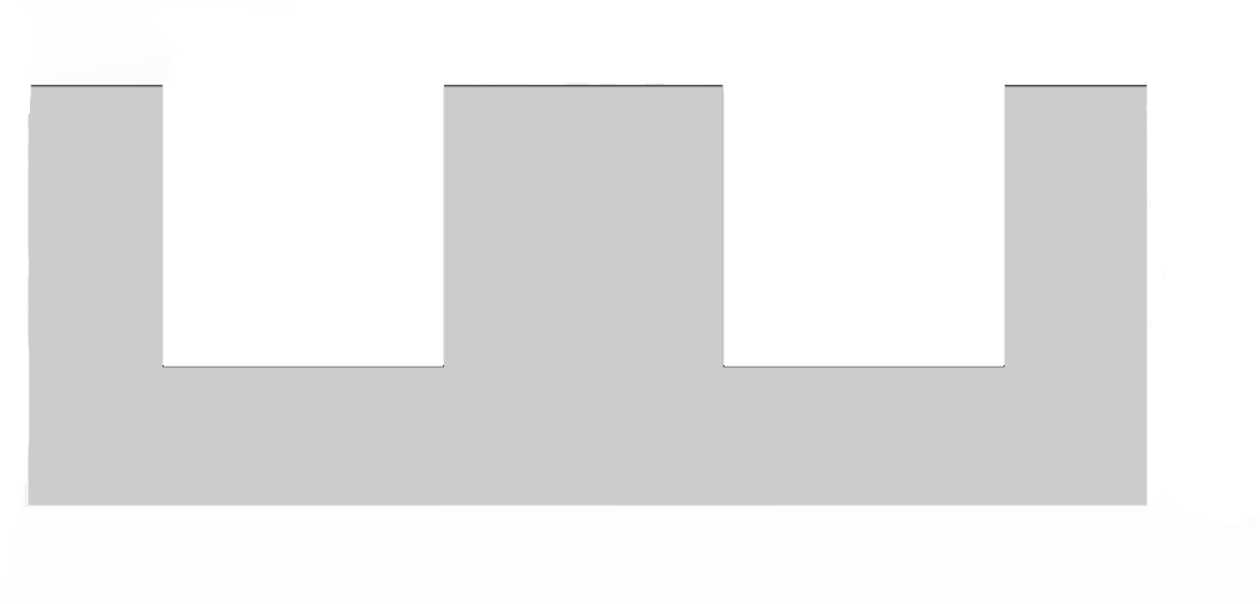

Figure 16 Diagram of RIE dry etching, grey is silicon and the darker grey is a thin layer of chrome.

Dry etching uses a concentrated plasma beam to blast away material from the sample. Reactive ion etching (RIE) is the most common dry etching technique. If a photoresist is used as a mask then during the etching process some of the resist will melt and harden to the walls of the etched area. However, if a metal mask is used then this melting does not occur. **Figure 16** depicts the end result of the RIE process when you use a thin metal mask. Since this technique is a highly anisotropic process it allows for a high level of precision. Dry etching has many advantages. It is not prone to contamination due to the process being conducted inside of a vacuum-sealed chamber. This allows for a higher degree of control which results in a far more repeatable process. It is also an easy process to start and stop which allows for quick changes if something goes awry. The biggest disadvantage is that this process is far more expensive than wet etching. Within RIE processing there are a number of pre-made recipes that users can start with that allow etching from nanometers to micrometers per minute. Slower etching rates allow for higher levels of control, as

well as the ability to create smoother vertical walls. However, as the etching rate goes up, as with the Bosch process (which can etch up to 5 μm/min), the walls will begin to taper and warp.

1.6 Slurry

When mixing dry powders into liquid, four properties must be taken into consideration, wetting, submerging, dispersing, and dissolving [79]. Wettability is the ability of the powder to absorb the liquid between all the different particles and pores. Sinkability, or submerging, is how well the particles sink into the liquid or float on top. This is affected by size, surface area and weight of the particles. Dispersing refers to the ability of the powder to disperse into the liquid on its own. If the dispersability is too low, then the addition of a dispersant can be added to speed up the process. Dissolving, refers to how well the powder mixes into the liquid and creates a more homogeneous mixture of the liquid and solid.

1.7 Controlling morphology of metals and ceramic powders

Understanding the morphology of powders that are created by each method is an important aspect of studying hydroxyapatite (HAp) [80,81,82]. For example, different morphologies can have various effects on, the cells of a living organism that the HAp medical devices come in contact with. Studies by Zhao *et al*. [83] explored the possible toxicity of variously shaped HAp, particularly needle, plate, rod and spherically shaped nanoparticles. From observations of which shapes caused the higher percentages of cell deaths, it was found that needle and plate shapes had a higher cell toxicity compared to sphere and rod shapes. Cell death was found to be closely related to the production of inflammation cytokine IL-6. Thus, controlling the powder morphology is a way to regulate how a material functions, improving or worsening its biocompatibility [84, 85].

Typically morphology is controlled through a number of ways. This includes the types of additives used, the pH levels, the solvents, pressure, reaction time, and temperature. These can all affect how a material is formed.

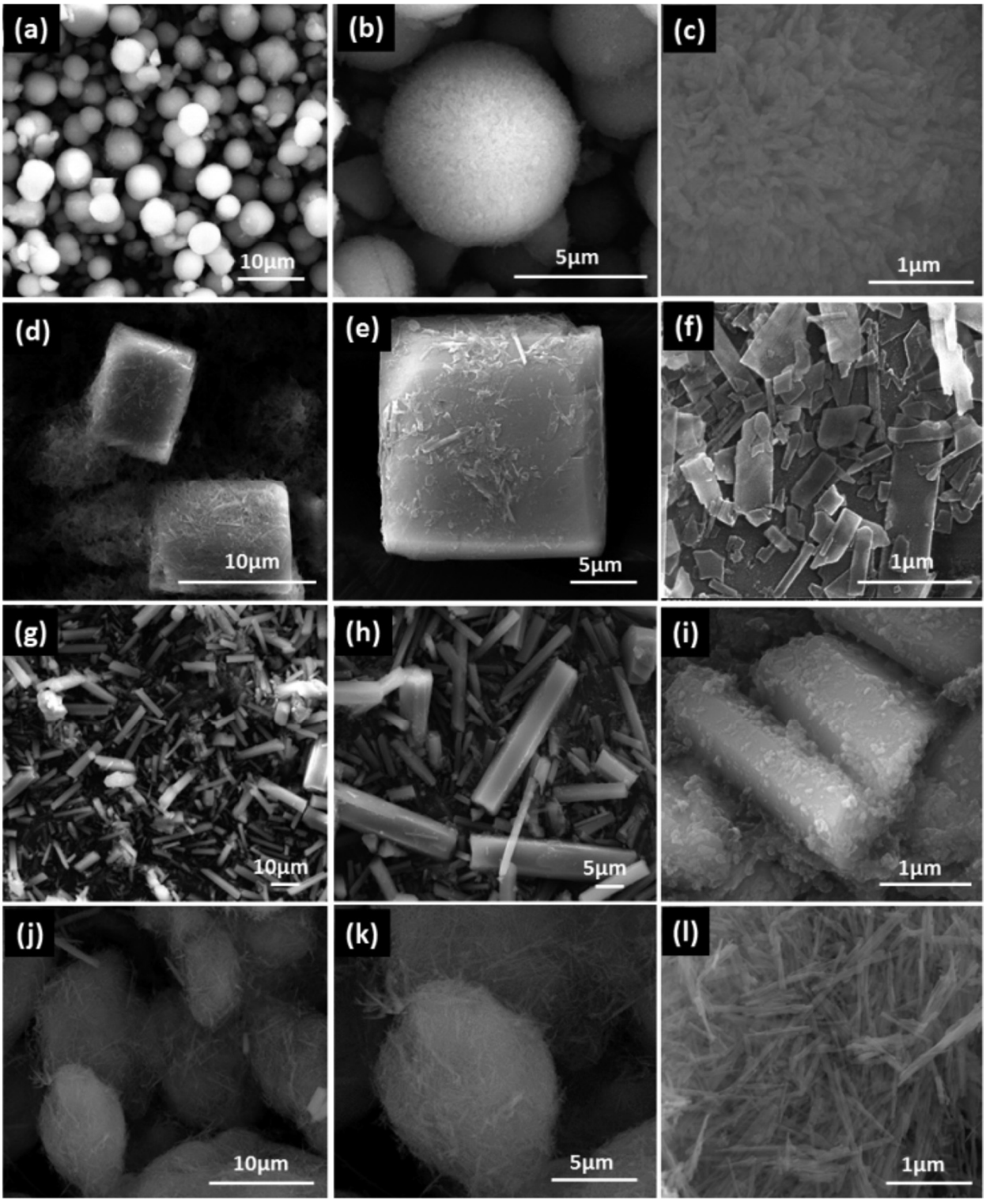

Figure 17 FESEM images of HAp with different magnifications of (a-c) spheres, (d-f) cubes, (g-i) hexagonal rods and (j-l) nested bundles (reprinted with permission) [28].

Research by M. Reeta and her team demonstrated how one material, in this case hydroxyapatite can have its morphology controlled to create numerous different types of shapes, specifically spheres, cubes, hexagonal rods and nested bundles, all from their nanoscale precursors. **Figure 17**, seen above, summarized the main shapes of HAp produced by hydrothermal methods by using different types of additives, pH levels, and solvents. Changing the additives, pH, and solvent of each reaction system, without changing the sintering process, led to the development of the various morphologies. The hydrothermal process shows great potential in forming other shapes because it allows for the control of the composition and size of the powders under specified conditions.

1.8 Macro scale morphology control

Figure 18 (a) Boing 747 in flight [86] **(b)** model kit of Boing 747, [87].

Previously stated methods of morphological control are used to control the shapes of materials at the nanometer and small micrometer scale. Shapes can be precisely controlled at the larger macro meter scale as well. All around society from planes, trains, and skyscrapers, to pens,

toys and lab equipment, the shapes of objects can be controlled via molding and casting. This can be seen in **Figure 18** where in **(a)** full size Boing 747 is shown which measures 232 feet, compared to **(b)** a 1 foot model of the same plane. Molding is the process of creating a shape from a liquid by using a rigid frame called a mold. A liquid material is then poured into the mold, in the form of plastic, metal or other liquid solution. Once heated and solidified, the material that is left inside of the mold is known as the cast. Numerous types of molding exist. These include blow, compression, extrusion, injection, laminating, and thermos molding. Each type of molding technique is best suited for certain sizes and materials.

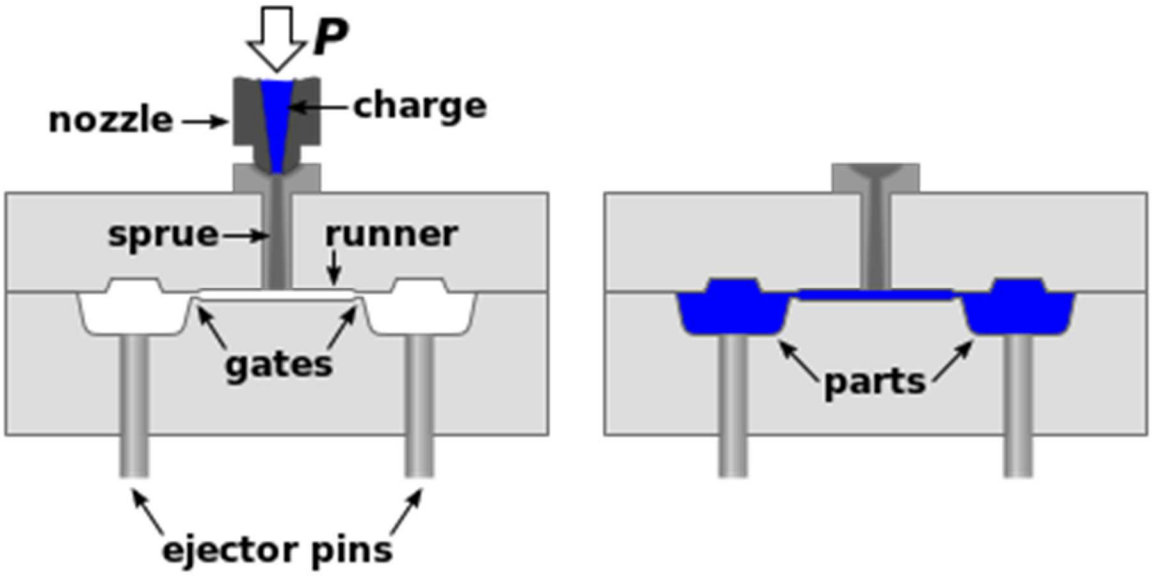

Figure 19 Diagram of injection molding process [88].

Figure 19 demonstrates injection molding. The material is initially injected inside the mold to fill it. Injection molding is used for metal casting, die casting, as well as plastic and polymer casting. In injection molding, a liquid, usually a metal or plastic, is poured into a mold that is closed off. The liquid is then allowed to completely cool. Once cool enough, the mold is taken

apart and the completed structure is removed. Polymers are commonly used because they have relatively low melting points, generally less than 300°C. This makes melting and cooling the plastic easier than metals or other materials.

The most basic form of molding and casting is the creation of simple geometric molds that then have a liquid solution poured into them. The mold is then sintered and the shapes removed. This can be most commonly seen in cooking, particularly baking, when creating cakes, muffins, and other geometrically shaped pastries.

1.9 Current study of morphology of powders, and motivation for research

Morphological change of powders is usually achieved through changing temperature, reagent concentrations, pressure, and reaction time. However current study looks to control the morphology of HAp without using these typical methods of morphological change. For this, we have turned to patterning on a silicon substrate, a method primarily used to create integrated circuits on semiconductor materials. This process involves growing or applying layers of a material on top of the silicon substrate. The substrate is then etched via wet or dry etching. By doing this repeatedly with different materials, circuits and other devices can be made.

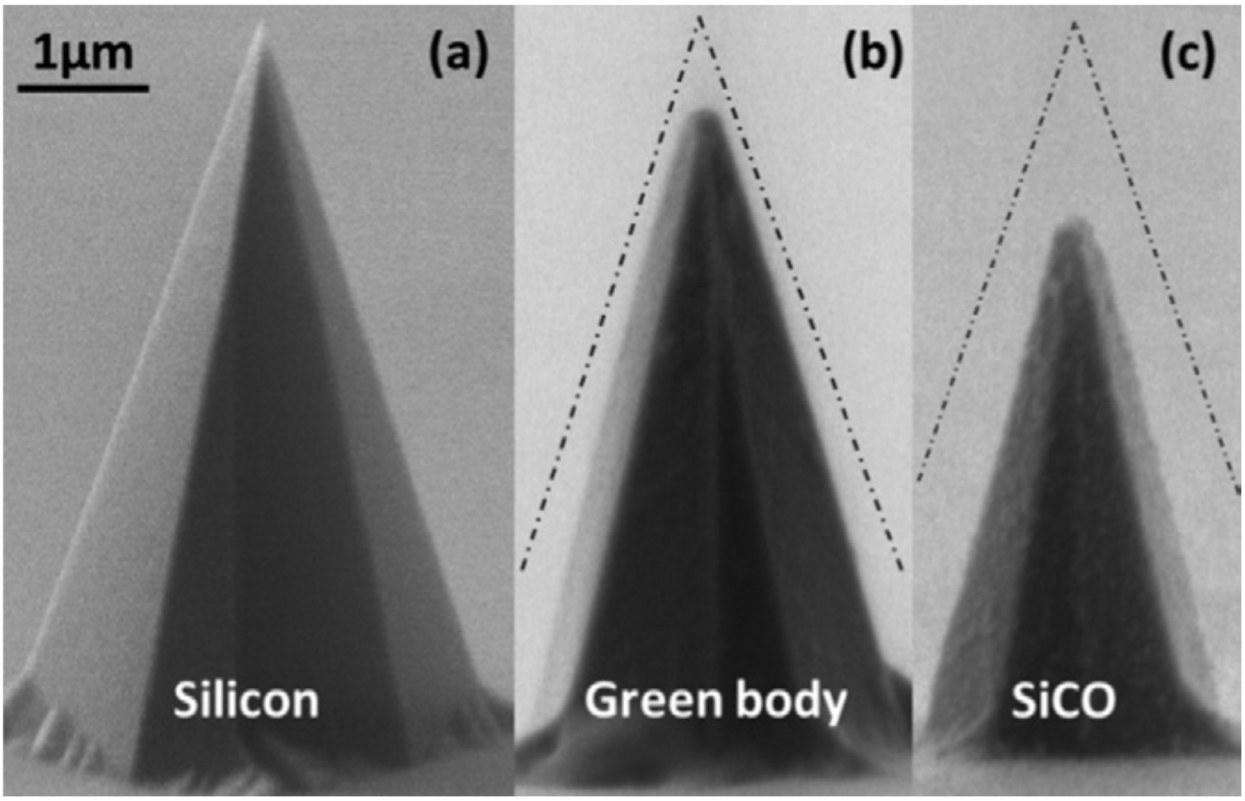

Figure 20 SEM images of nano-tipped ceramic needles attached to a substrate, (reprinted with permission) [107].

There has been extensive research into micrometer scale molding. Current industries have a strong desire to reduce the size of present machines and devices. This is a pattern found in many fields of science; the desire to miniaturize devices from satellites to body implants. Thus the majority of work into micrometer scale molding and casting has involved creating films, optical lenses [89].

Previous studies were found that created molds and cavities that were similar in precision needs, but used vastly different processes to caste their desired material. The research that most closely resembled our own was research by Grossenbacher. Micrometer scale, nanometer tipped needles for medical application were produced via molding and casting. Results showed the successful creation of needles with bases roughly 3µm in diameter and tips that reached several nanometers in diameter. **Figure 20** demonstrates the creation of the nanometer tipped needles in

its three stages of development, silicon, green body, and SiCO. Silicon molds were used to caste their material. A major difference in their project was that the needles were attached to a larger ceramic substrate. Thus after the material was sintered the needles were not individual pieces, but as features on a larger ceramic surface.

In this study we combined both patterning on a substrate and HAp powder to produce micrometer sized HAp cylinders for prospective biomedical applications. We first produced micrometer scale, densely packed, cylindrical shaped cavities with smooth walls that are 5μm deep and 5μm across by photolithography and waveguide etching techniques on a Si substrate. The cavities were filled uniformly with HAp slurry, and sintered. Next, the sintered specimens were removed from the cavities, and characterized by SEM. The corresponding specimens of sintered HAp resembled the molds in which they were cast. Shapes after removal from their molds were all very similar in size and shape. The presented technique demonstrates a great potential for forming large amounts of identically shaped, microscale samples of HAp, or other similar ceramics, for potential biomedical applications.

This project stands apart from any published work in a way that the desired shapes were not sintered being attached to a larger surface; this allows producing individually shaped structures. While traditional methods of morphological control can produce numerous shapes and sizes, homogeneity is still one of the biggest problems. 10μm sided cubes can be created by hydrothermal method, as seen in research by M. Reeta. However, there are errors involved which prevent the cubes from all being the exact shape. The current project looked into the possibility of creating shaped structures that were identical in not only their shape, but their size as well. The main goal of this work was to show that it is indeed possible to control the morphology of a ceramic at the micrometer scale, rather that the nanometer scale, as it is usually explored with powders.

In particular our approach of pouring solutions into the cavities, instead of inundating the entire substrate, then removing them from the cavities is different from most projects. It is a unique approach to controlling morphology of sintered powders that's sets it apart from other research done to explore micrometer molding and casting.

2. Experimental Procedure

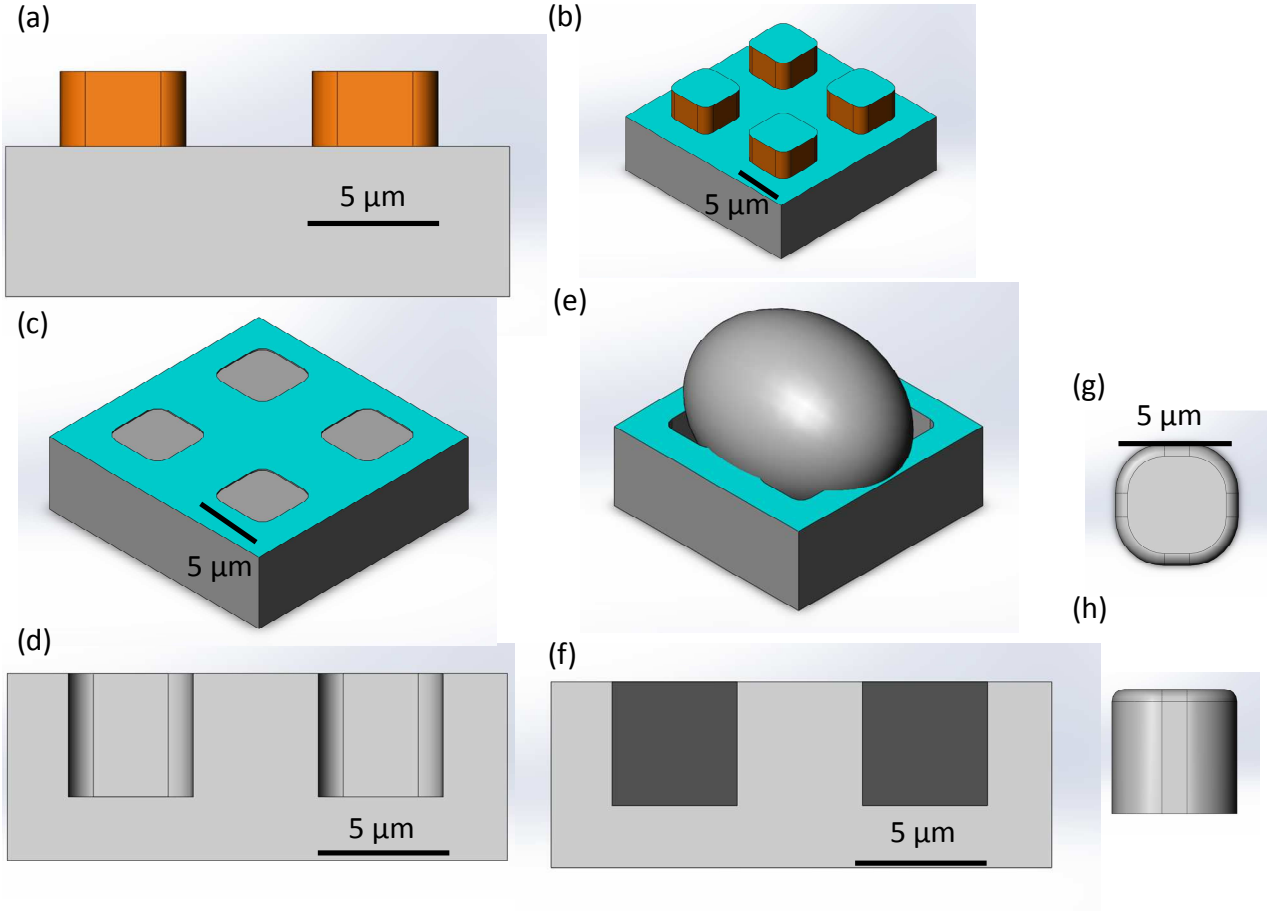

Figure 21 A detailed fabrication route of cylindrically shaped HAp samples: **(a)** photoresist patterning with metal deposition side view, **(b)** photoresist patterning with metal deposition angled view, **(c)** lift off process angled view, **(d)** etching process side view **(e)** slurry creation and drop wise method application **(f)** side view of filled cavity **(g)** top view of finished sample, **(h)** side view of finished sample, produced using Solidworks.

2.1 Fabrication of Silicon Mold

The detailed fabrication route of cylindrically shaped HAp samples is illustrated above in **Figure 21**. The project started with a set of 25 wafers from Helitek Company Ltd. (Freemont, CA) Wafers were 500-550 µm thick and 4µm in diameter. Before testing began on the wafers,

additional steps were taken to ensure cleanliness of the wafer samples. Wafers were placed in acetone baths and dried with an N□ gun. Wafers were then given a 20 minute oxygen cleaning to ensure any remaining organic material was removed.

A 5-inch square quartz photomask was procured from Front Range Photomask LLC. (N. Lake Havasu City, AZ) **Figure 22** shows the digital rendition of what the design of the photomask was designed to have. The quartz mask was purchased with a thin layer of chromium on one side, containing 5 x 5 μm shaped gaps with 1 μm rounded edges. The squares had these rounded edges due to the limitations in resolution quality. Each square was distanced 10 μm apart from center to center. **Figure 23** shows what the square shaped gaps of the photomask look like under an optical microscope.

Photolithography is the first step of sample processing (**Figure 23a**). During this step a 5-inch, chrome/quartz photomask was used. Negative photoresists were used in order to create cylinders that were 3 μm in diameter and 5 μm in height across the wafer.

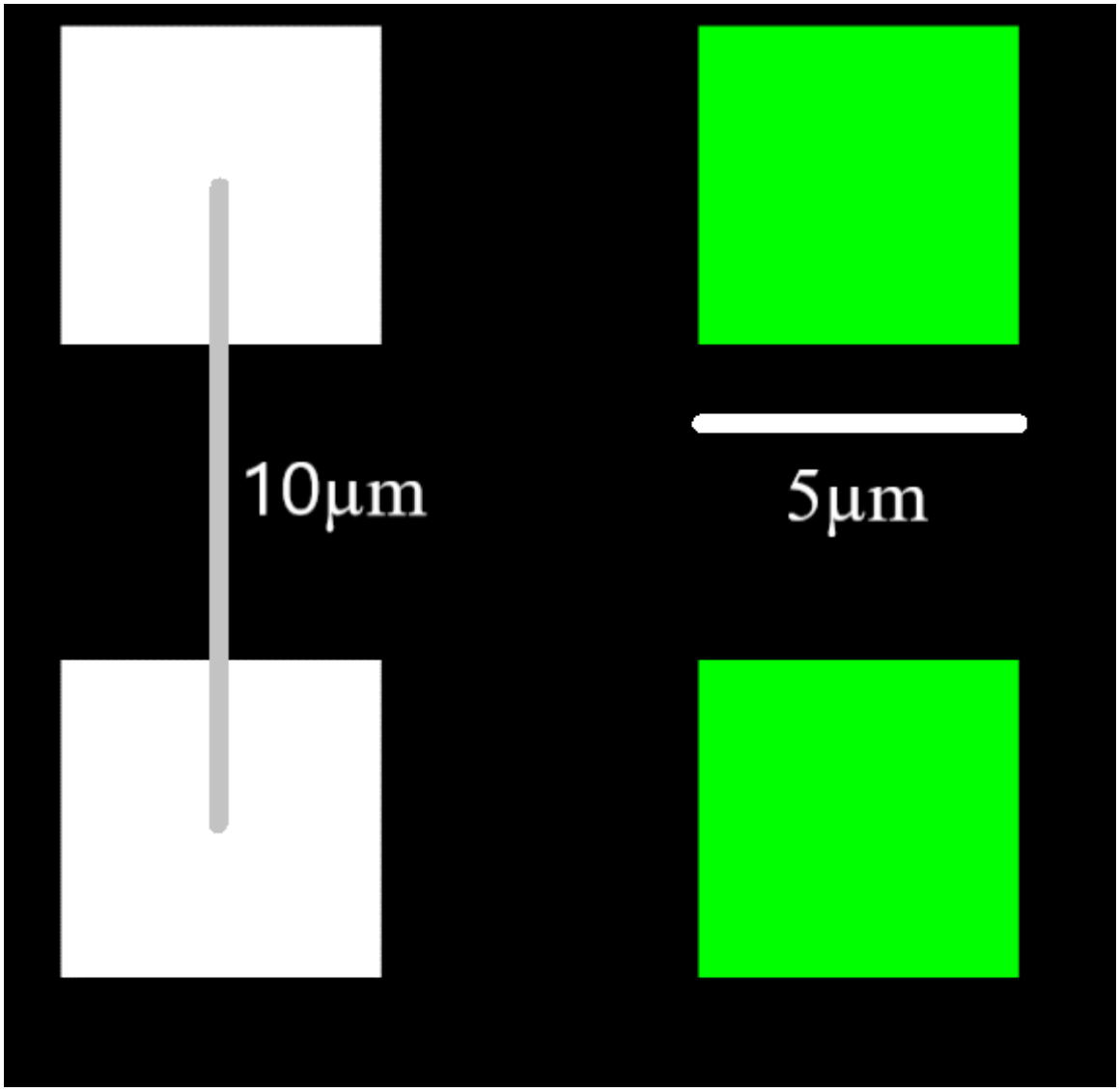

Figure 22 Original design of photomask.

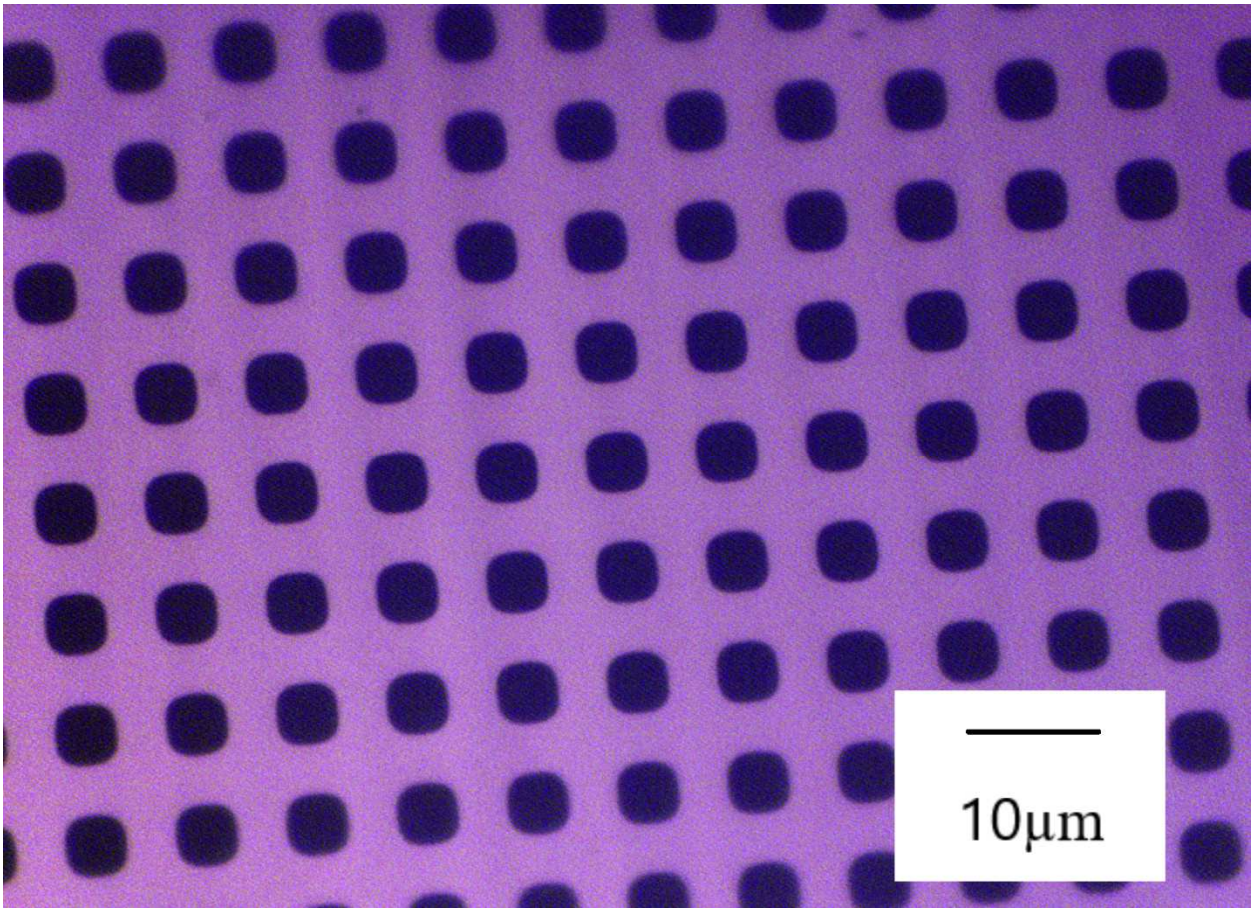

Figure 23 Optical microscope image 20X of photomask pattern.

After cleaning, the initial stages of photolithography can begin. The wafer was placed on a hotplate at 150°C for 10 min to evaporate any residual moisture on the surface. NR9-3000PY negative photoresist was squeezed onto the wafers' surface by a pipette. The spin coater was set to 3000 RPM for 40 s. Once completed, the sample was placed on a hot plate at 150°C for 1 min for what is known as the soft bake. The sample was then placed into the resist exposure device. Resist exposure was conducted using an MA6 Mask Aligner (Karl Suss, Garching, Germany), which shines concentrated UV light at 11 mW/cm^2 and wavelengths of 365nm, although this particular machine can go between 350 and 410nm. The device was set on hard contact mode to maximize resolution. It is better if the machine can be set to vacuum contact mode to increase resolution, however our machine did not allow this for the size of our wafer. The mask was oriented

by placing the chromium patterned side against the wafer. The sample was exposed for 40 s. The sample was then placed on another hot plate, this time set for 100°C for 1 min, for what is known as the hard bake. Once completed, the sample was placed into a dish filled with RD6 developing solution (Futurex Inc., Franklin, NJ). Enough solution was used to cover the wafer. The sample was developed for 17 s. After 17 s the sample was removed from the dish and subsequently rinsed thoroughly with deionized water for roughly 10 s, then dried completely using an N□ gun.

During the initial stages of the process it is important to check the thickness of the photoresist to ensure the correct photoresist thickness is reached. This is done after soft baking the sample. The wafer was placed under a Filmetrics F20 (Filmetrics, San Diego, CA), to measure the thickness of the photoresist. Once the proper thickness has been achieved it is necessary to make sure that pillars were created during the process. Verification of proper photoresist pillars was done after developing the sample in RD6. This was accomplished by using an optical microscope that had zoom capabilities from 20X to 100X. There was also a color contrast between the resist and substrate. The photoresist appeared much darker than the silicon due to the optical properties of the substance.

Once the verification of pillars is confirmed, metal deposition can begin. A Denton Discovery 18 Sputter System was used to deposit a thin layer of Chromium (Cr) onto the pillars and surrounding areas. Normally metal deposition samples are rotated during the deposition to ensure an even deposition across the entire surface. However, by doing this, metal would then be deposited on the sides of the pillars which would make it more difficult to remove the photoresists and expose the silicon underneath. To avoid side deposition, the sample was set at an angle of 45° so that the substrate completely faced the Cr cathode. The rotational speed was also set to 0 so that it did not rotate. It is important to note that facing the sample towards the cathode increased the

rate of deposition by three times. The power setting was set to 200 W to enable a smooth later of Cr at a pressure setting of roughly 2.4 mT and gas rate of 33 sccm. Pressure and gas rate settings might vary slightly from run to run due to cleanliness of the chamber. The Cr was then deposited for 30 s at a rate of roughly 0.83 nm/s. This created a Cr layer of ~25 nm on top of the patterned wafer. This included the top of the wafer's surface, and the tops of the photoresist pillars, but not the sides of the pillars since the sides did not face the cathode.

To remove the photoresist pillars by the lift-off process and prepare it for dry etching, a dish was filled with enough RR41 resist remover (Futurex Inc., Franklin, NJ) so that the sample could be completely submerged. RR41 performs like a weaker form of acetone, thus it removes the photoresists without stripping the Cr. The dish with RR41 was placed into an ultrasonication device. The sample was then placed inside of this dish and submerged and ultrasonicated for 25 s (longer than 25 s begins to remove the chromium as well). During the lift-off the removal of the resists was somewhat visible. It appeared as a dark liquid coming off of the sample; the liquid was usually visible until the 15 to 20 second marker. Once the lift-off process was completed, it was pulled out of dish, washed thoroughly with deionized water and dried with an N□ gun. If it appeared that large chunks of Cr were coming off during the washing process or even during the RR41 bath, then the sample had been submerged for too long and would need to be restarted from scratch. It was very important to not submerge the sample for too long, as removing extra Cr diminished the useable area on the wafer. Once lift-off was completed, square-like openings onto the silicon were left where the photoresist pillars had been. These openings were in turn surrounded by chromium which act as a hard mask for the dry etching step. The end results of this process is seen below in **Figure 24**, and **Figure 25**. **Figure 24** presents a further shot to give a bigger perspective of what the wafer looked like after lift-off. Areas where photoresists were removed are

now darker than the surrounding areas. When looking closer, **Figure 25**, it is shown how these darker areas are indeed shallow holes that are roughly 25 nm in depth.

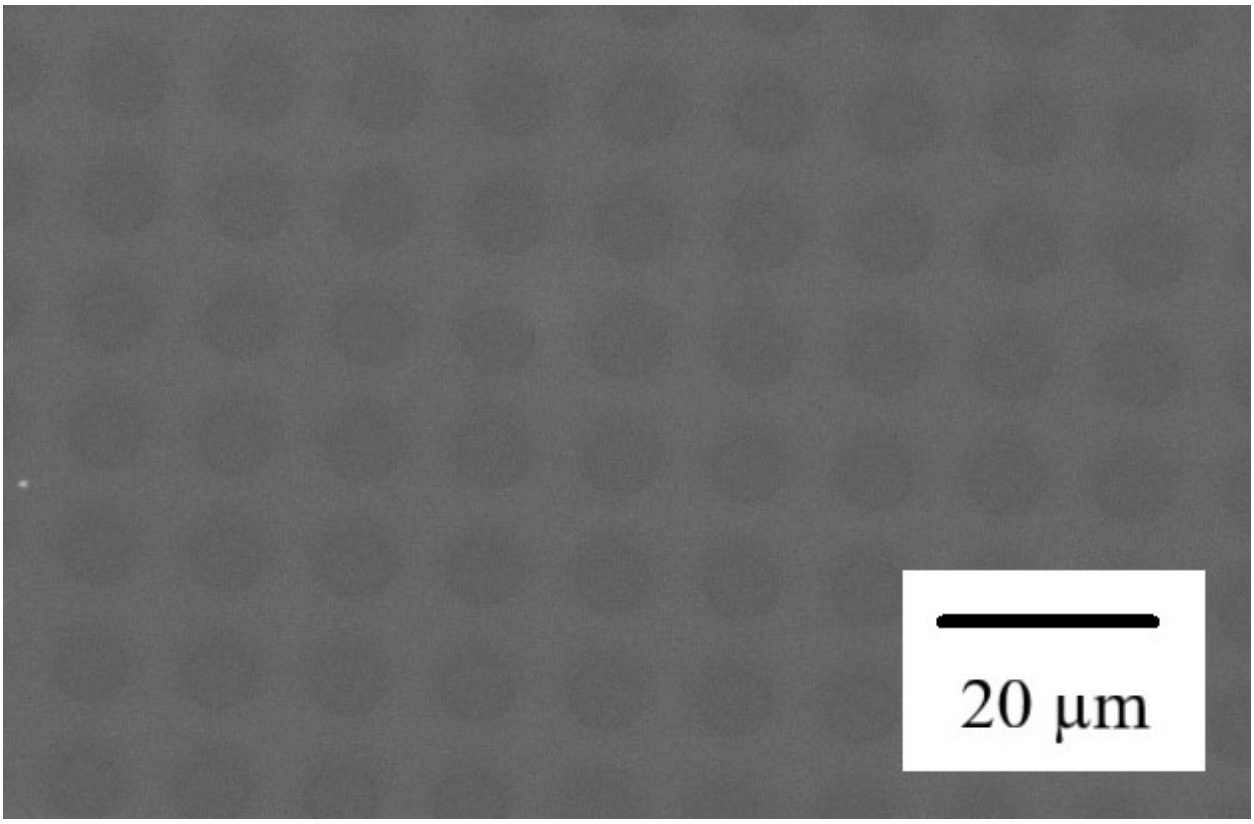

Figure 24 SEM image of wafer sample after photoresist pillars have been removed, known as post lift-off process.

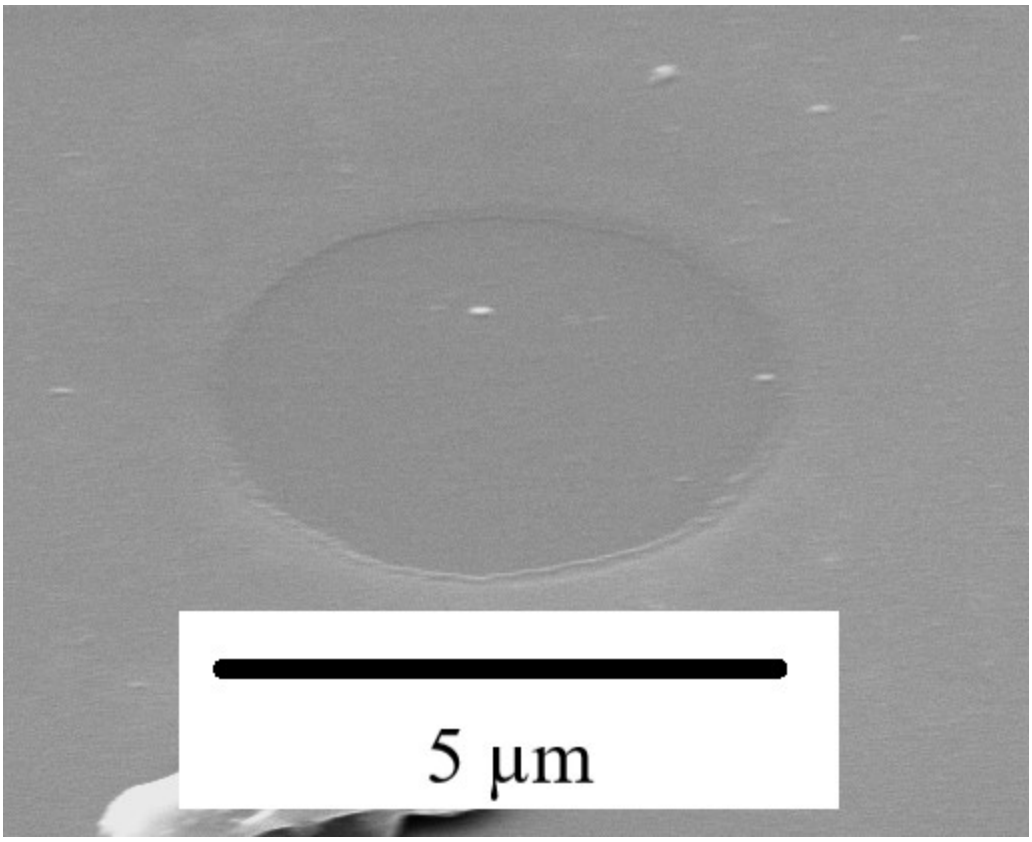

Figure 25 SEM image of post liftoff, the small hole can be seen where photoresist pillars used to be, along with the 25nm of Chrome around it.

In order to verify the lift-off process, the sample is viewed under an optical microscope at 50X or more. Due to the slight difference in depth between the lifted off photoresist versus the Cr mask around it, about 25 nm, the coloration between the two are very similar. However, upon closer examination at 50X or more, the slight coloration changes between the Cr and Si are more noticeable. The bare silicon holes appeared darker than the silver coating of Cr around them.

The last step in the microfabrication process entails dry etching to create 5 µm deep cavities. The sample was loaded into an Oxford Plasmalab 100 RIE/ICP (Oxford Instruments, Santa Barbara, CA). Silicon waveguide etching recipe was selected for use. Pressure was set to 17 mT at a flow rate of 8sccm, and was etched for 20 min at a rate of 0.25 µm/min. Dry etching in this case etches the silicon much faster than the chromium. Risk of cross-contamination was a

major concern when conducting the etching process. If the flow rate jumped to a high number, in particular 60 sccm or more, then the sample was leaking heavily. These heavy flow rates give credibility to the possibility of cross-contamination occurring inside the chamber and was the most likely the cause of this. In order to develop a repeatable method to fabricate these molds, experiments were conducted to determine the etch rate, by keeping the power setting constant and experimenting with time to determine what etch rate was used. Etch rate is highly impacted by the amount of surface area being etched, the size of the cavities and the power settings for etching [90,91]. The listed rate for silicon waveguide etching is 0.5 μm/min, however it was found that the actual rate was 0.25 μm/min. Therefore, silicon waveguide etching was conducted for 20 minutes to achieve the desired depth of 5 μm. Once etching was completed, the entire surface of the wafer was covered with cylindrically shaped cavities that measured 5 μm in diameter and 5 μm in depth. Etching was successful when the then cavities were visible under the microscope. Cavities were seen as dark holes surrounded by a very light material. This was seen most easily using a filter that showed the different heights as a different colors.

2.2 Creation of Slurry

To create the final cylindrical HAp powders, the cavities were filled with slurry of deionized (DI) water, HAp powder (Sigma Aldrich, <200 nm particle size (BET), >=97% purity, Lot #MKBP3048V, 677418-25G PCode 1001566643), and Darvan 811 Dispersant (Vanderbilt Minerals, LLC, Norwalk, CT)(sodium polyacrylate, product number 14255). Two drops of Darvan 811 were added to 700 mg of DI water. Two drops of 811 were added to the water drop wise via a DLS pipette which dispensed the liquid at a consistent 13 µl per drop. Next, 500 mg of HAp powder were slowly added to the water/dispersant solution shaking the liquid in the process to help the powders dissolve. After the powder was added, 30 additional drops of DI water (which was about 1100 mg) were added to the solution using a 3 mL pipette. Finally, the solution was ultrasonicated for 10 min, removing it from the ultrasonication bath once per minute to manually shake the solution and ensure the bottom is mixed well.

Before filling the cavities with the liquid solution, the 4-inch wafers were diced up into smaller parts, roughly 0.25 to 0.5 cm^2 in area. However, the exact size can vary, as long as the pieces of wafer can fit inside of the crucible.

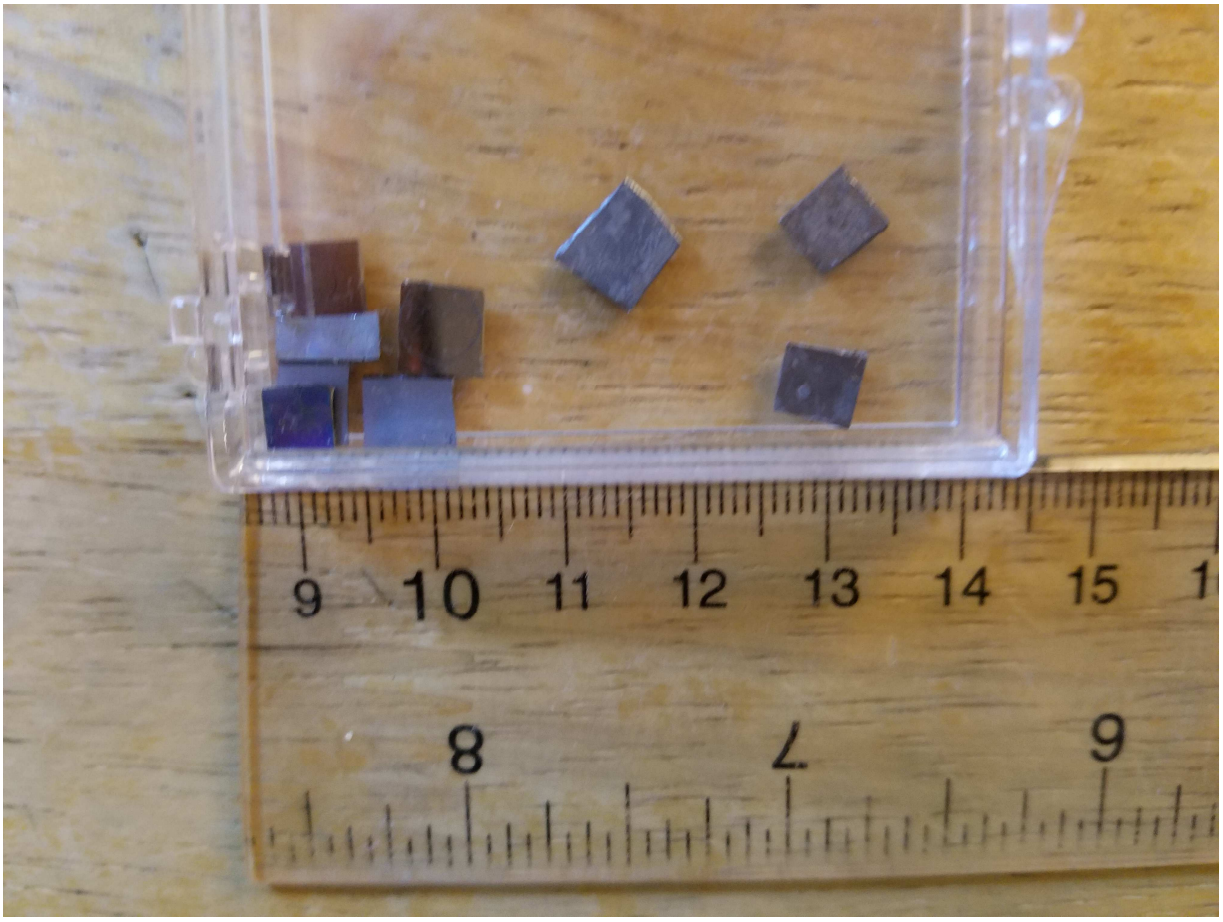

Figure 26 Image of diced silicon samples of varying sizes from ~0.25 to ~0.5 cm^2.

Dicing samples was easy because only a diamond tipped cutting tool is needed. It is very important to be wearing clean, non-textured gloves during the dicing process. Textured gloves leave smudges on the surface of the wafer sample and would require it to be cleaned again. **Figure 26** shows an image of different wafer samples alongside a ruler to give an idea of their general dimensions.

Figure 27 Image of slurry drop on top of Si substrate.

Liquid solution was dispensed onto the surface of the substrate via a small pipette. We used a extended fine tip transfer pipette, from Samco Scientific, since they were able to dispense the smallest amount of liquid while being consistent in volume from drop to drop. However, larger pipettes could be used as long as drops were not so large that they cover much of the surface of the sample.

When filling the pipette with the solution the tip of the pipette touched the bottom. This is important because since ceramics are not very soluble they began to settle down quickly. Thus filling from the bottom ensured that the solution would have as much of the ceramics in it as possible.

Several diced samples were placed on a tray that was put inside a vacuum tube. One to four drops, depending on size of substrate, were placed onto each sample that was being prepared. The goal was to place enough solution to cover as much of the surface without causing the surface tension to break, causing the liquid to spill off of the sides. **Figure 27** shows roughly how much liquid solution should be placed on a sample. Once completed, the tray was placed inside of a vacuum chamber and the pump began to pressurize it. Drying time was variable because it depends on how many samples are drying at once. One to ten samples took approximately 30 to 40min, 60 to 100 samples took 4 hours or more.

Figure 28 Image of slurry dropped after it has been dried.

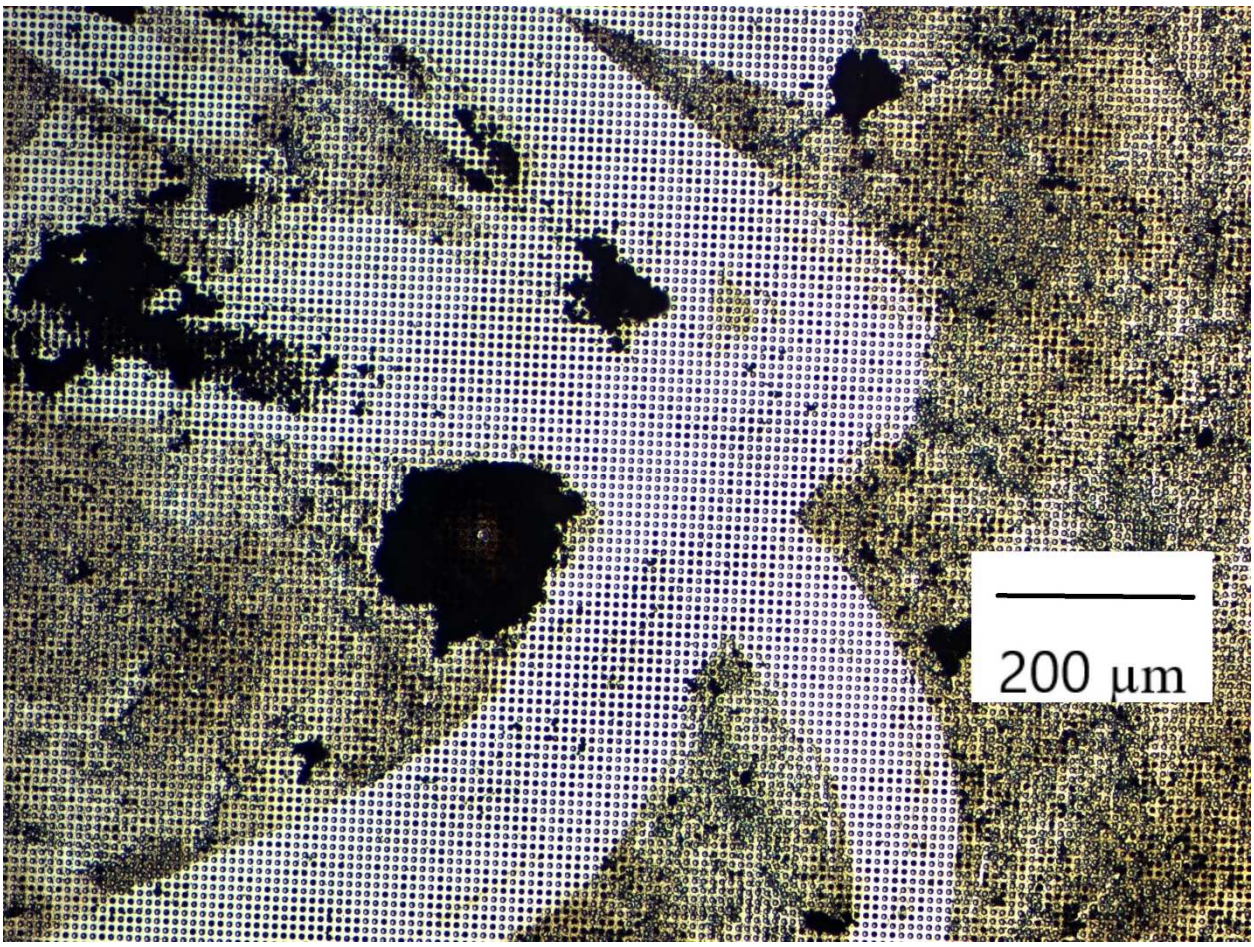

Figure 29 Optical microscope image at 10X, showing areas of substrate that have been scrapped [lighter parts] versus areas that are not scrapped [darker parts] after drying.

Once fully dried, the samples were removed from vacuum chamber and the excess ceramic was scraped off using a set of plastic tweezers. This removed excess material stuck to the surface, as well as overfilled cavities, without scratching and damaging the substrate. Sometimes some of the remaining Cr mask was removed but this was okay since no more etching was necessary for the samples. **Figure 29** shows an optical image of what the sample looks like with areas of excess material removed, and areas that have not been removed. It is easy to see how effective the removal process is. Removing the excess material is important because there will be less excess and waste material upon removing the cylinders later after sintering. This makes it easier to find complete

and unbroken samples. After removing excess material, the samples were placed in an alumina crucible or plate/dish, or crucible of equal strength that is able to withstand temperatures up to 1300°C. **Figure 28** shows what one dried sample may look like before removing the excess ceramic on top.

2.3 Sintering Slurry

Figure 30 Post sintered alumina crucibles and dish.

Diced samples were placed inside of alumina crucibles or dishes and put in a high temperature furnace. Samples were sintered at 1250°C, with heating and cooling rates set for 5°C/min, and held for 2 hours at 1250°C [92,93,94]. Several sintering temperatures between 700°C and 1250°C were tested in order to find what temperature would produce the densest cylinders. If

using a dish or tray, be extra careful when handling them as they can break very easily. Samples were allowed to reach room temperature before removing from the furnace. **Figure 30** is an image of the different sized alumina crucibles and dishes that were used to sinter the specimens.

2.4 Extraction of Samples

After sintering, the samples were removed from their cavities. Sintered specimens were placed upside down inside of a small beaker. We used 25 mL beakers. Enough acetone was squirted inside the beakers to cover the samples. Acetone was chosen over water for several reasons. One, acetone dries far faster than water, so this sped up the experiment greatly. Two, since acetone dried so much faster, agglomeration of the particles during the drying phase was minimized. Finally, there was little to no outside contamination in the acetone solutions compared to water solutions. Water was initially tried as a liquid suspension for the HAp, however there were several disadvantages to it. Samples were subsequently ultrasonicated for 5 min. During the ultrasonication process the sample was removed once a minute and shaken around manually from side to side to assure solids were not amassing at the bottom in the form of white sediment.

2.5 Characterization of sintered samples

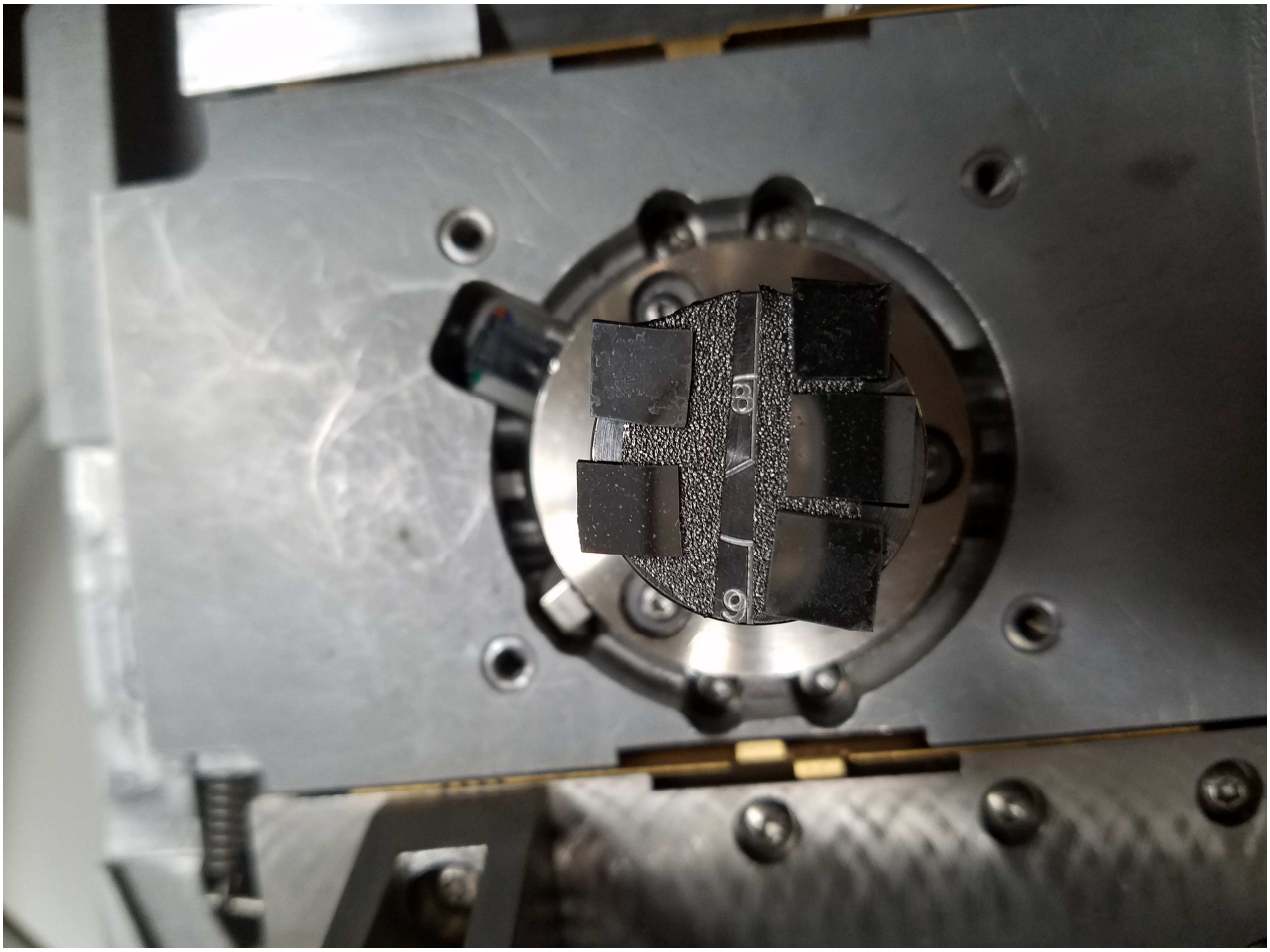

Figure 31 Prepared samples on blank silicon substrates for SEM imaging.

The corresponding cavities and samples were subsequently characterized by optical microscopy at magnifications from 5X to 50X and scanning electron microscopy (SEM) (FEI-XL30, FEI Company, Hillsboro, OR) using 10kV accelerating voltage. For SEM imaging, all samples were placed on bare Si substrates, mounted on aluminum sample holders and sputter-coated with a few nanometers of iridium. As seen in **Figure 31**, drops of the extracted material solution were placed onto bare silicon substrates and allowed to fully dry. Samples were initially mapped out using optical microscopes to find areas of the sample that appeared to be promising and were subsequently viewed with SEM to either confirm or disprove the areas in question.

3. Results and Discussion

3.1 Fabrication of Cavities

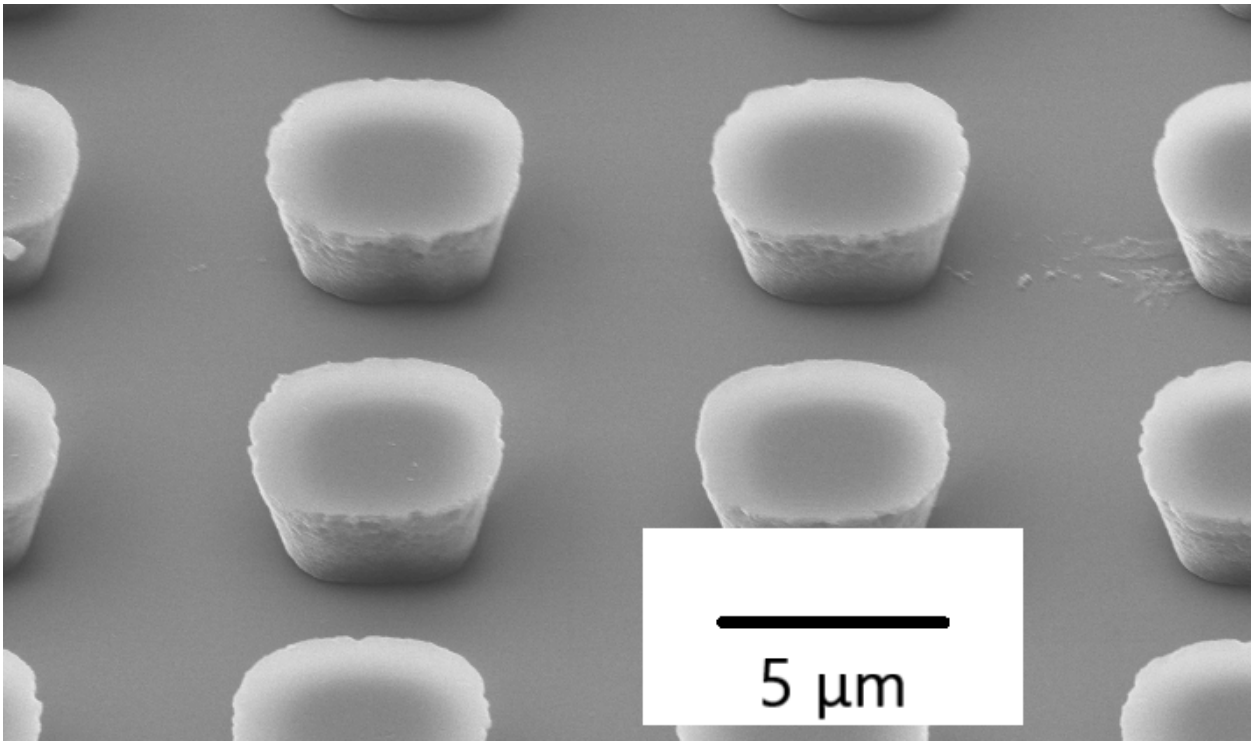

Figure 32 SEM image of photoresist pillars before Cr deposition and lift-off process.

To ensure that the cavities were properly formed, each of the above-mentioned experimental steps were verified to show they worked properly. Verification that proper photoresist pillars were created was the first step. As seen in **Figure 32** photoresist pillars were correct in shape and size. The shape resembled a rounded cylinder. The tops of the pillars were not perfectly smooth. They appeared rough as seen above, but this did not matter as the bottom of the pillars was what formed the outline of the etched area. On the other hand, the bottom parts of the pillars indeed had straight edges with rounded corners that were about 5 µm in height. With verification of the photoresist layer complete, metal deposition and subsequent lift-off processes could commence.

To determine how to create proper looking pillars experiments were carried out at various exposure times from 10 to 50 seconds, using Nano3's MA6 mask aligner. The machine was setup so that the dosage output was 11mW/cm^2. Due to the nature of negative photoresists, undercuts form from the exposure dose. Higher doses minimized this undercut, but it was very difficult to completely remove it. Since negative resists form this undercut, it made this resist perfect for lift-off process. Undercuts make it harder for metal to be deposited over the entire surface. Various times were used to find a dosage that would minimize the undercut, so the lift-off pattern would be close to the original size without causing oversaturation. Large changes in the undercut angle were viewed from 10 to 30 seconds. After 40 seconds the undercut did not noticeable change. Thus, 40 seconds was the chosen dosage time, which resulted in a dosage of 440mJ.

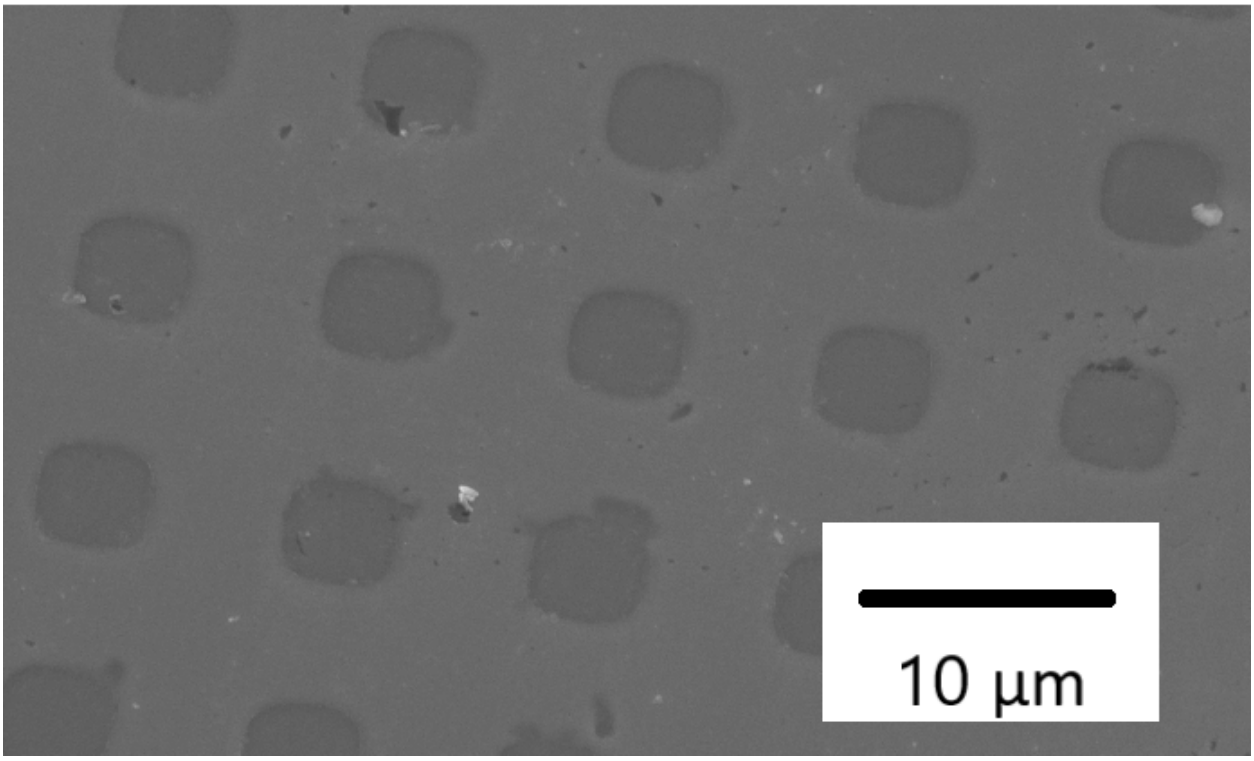

Figure 33 SEM of mid-range shot of post lift-off process.

Verifying the lift off process was the next key step. As seen in **Figure 33** pillars were successfully coated in Cr and removed via RR41 resist remover. The exposed areas of silicon

indeed look like the original photomask, with some imperfections. Also in **Figure 33**, straight edges can be seen in the image with rounded edges, the show the outline of the cylindrical shapes that will be etched into the wafer. Most of the openings to the silicon look good, except for small specks of Cr mask missing here and there. Any parts of Cr missing are most likely due to the lift-off process in RR41. As was stated earlier, if the sample is allowed to stay in the RR41 for too

long, not only will all of the photoresist be removed but chrome will begin to be removed as well since the Cr which is deposited is not bonded strongly to the silicon substrate.

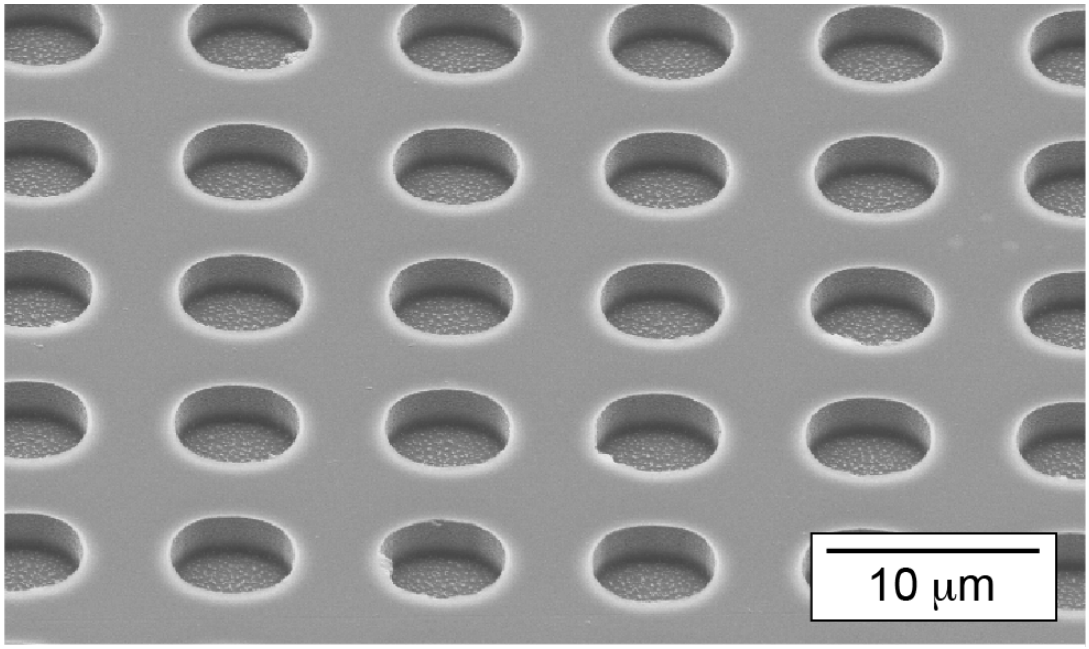

Figure 34 Scanning electron micrograph of mold for the manufacturing of the HAp cylinders.

SEM micrograph (**Figure 34**) show that photolithography and etching were successful. **Figure 34** shows how cavities with smooth walls were created with dimensions of 5 by 5μm. **Figure 34** also shows how the etching was uniform over a large area. Experiments were conducted to determine the etch rate, in order to develop a repeatable method to fabricate these molds. This was done by keeping the power setting constant and experimenting with time to determine what etch rate was used. Etch rate is highly impacted by the amount of surface area being etched, how large the cavities being etched are, and the power settings for etching [95,96]. We found the listed etch rate of 0.5μm, as stated by the manufacturer of the machine, was inaccurate. The actual etching rate was 0.25μm/min, therefore 20 minutes of etching was needed to achieve the depth of 5μm, as seen in **Figure 34**.

3.2 Creation of Slurry and Filling of Cavities

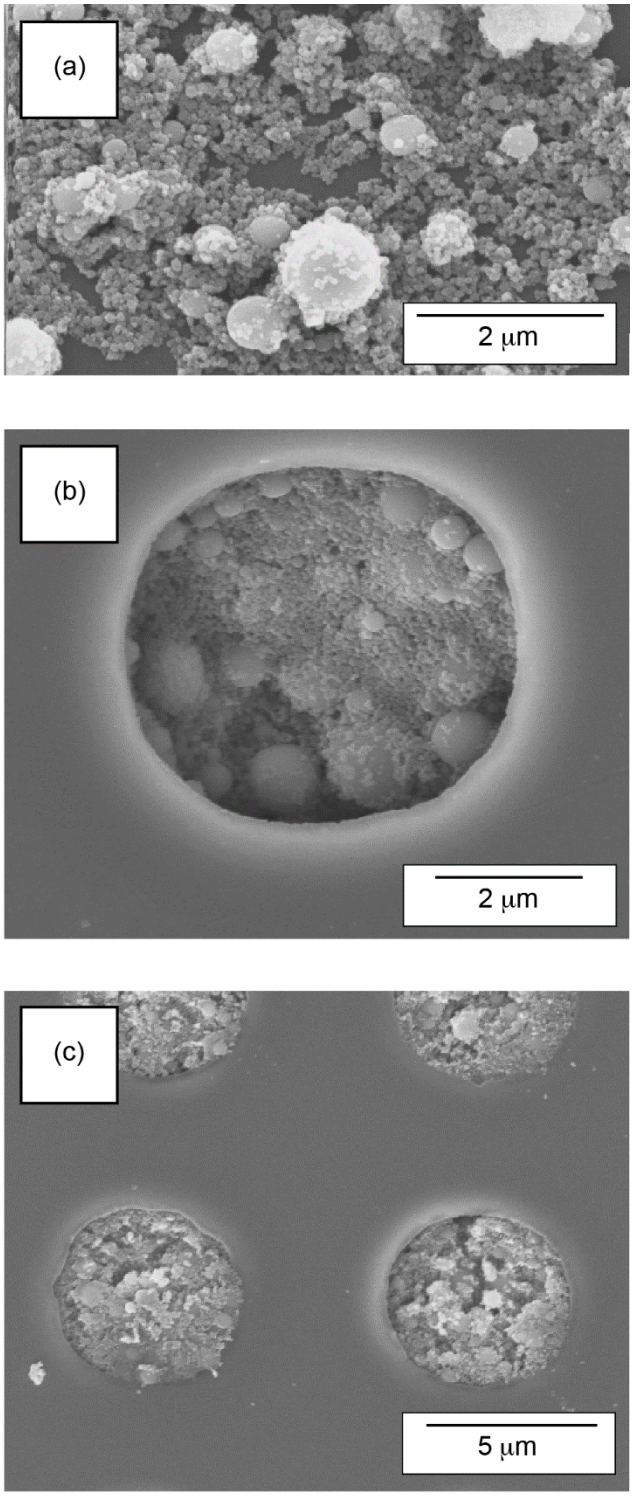

Figure 35 Scanning electron micrographs of (a) as-received HAp powder, and (b)-(c) cylindrical cavities filled with slurry before sintering. The slurry was not sintered yet, but dried for purposes of imaging.

In creating the HAp slurry, both the ratio of water to HAp to dispersant, and the mixing order were taken into consideration. Mike Frank et al. reported, the amount of dispersant needed per sample batch is 1.4% weight of the solid ceramics [97,98]. Frank also mentioned that this percentage merely represents the minimum amount of dispersant needed to achieve maximum dispersal. Adding more dispersant would have no additional dispersing affect. This agrees with results reported by Cheng and Kuhn who used dispersant equal to 1.67% weight of the ceramics in their experiments using calcium phosphate (CaP), a precursor to HAp [99]. Keeping these prior studies in mind, we aimed to keep the amount of dispersant low, adding just two drops of 811 [26 μL] to the water. It was found that each drop weighs ~13.8mg, and are equivalent to 5.52% of the weight of the solid materials being mixed. Dispersants were burned away during sintering process so they would not contaminate the results. **Figure 35** illustrates the morphology of the as-received HAp powders [**Figure 35(a)**], and several cavities containing dried slurry before sintering.

The end ratio of about 1821mg of DI water to about 500 mg of HAp was experimentally found to give the optimum slurry. Solutions with a high-water content proved to be far more effective in filling cavities while leaving little solution on the surface of the substrate, than did ratios that favored higher amounts of powder to water. Cavities were well-filled by the solution, and the slurry did not rise up on the sides, but was evenly packed inside, as shown in **Figures 35b** and **35c.** This was proven necessary to create the densest post-sintered results. **Figure 35c** also shows how before sintering very little solution was left on the surface of the wafers outside of the cavities. This point proved to be critical, since once the samples are popped out, whatever is left on the surface would be removed as well. Surface debris could mix in with the popped-out cylinders, making it more difficult to find pure cylinders, thus changing the quality of the overall yield.

The order in which the materials were mixed was also found experimentally. Mixing powder into liquid was found to be the most efficient method to promote a faster and more even mixing. It was found that mixing the powders into the liquid solution promoted less agglomeration, than if the liquid was mixed into the powder [100]. Performing the mixing in this order, coupled with using a dispersant, maximizes the speed of the wetting process. This created a well dispersed solution with minimum agglomeration and a high percentage of dispersability.

Figure 36 Image of droplet just past breaking the surface area point.

Various methods of dispensing or placing the solution onto the substrate were tried. This included multiple sized pipettes as well as submerging the substrate in the solution. The latter one was not effective, since both silicon and chrome are highly hydrophobic. The solution was in a liquid phase, rather than a slurry or smoothie-like consistency. Therefore it did not stay on the surface of the Si wafers during the submerging process. This was overcome by trying out different

pipettes to determine the correct amount of deposited material. If too much solution was placed on a sample, part of the solution would flow off of the sample, ruining that trial. This is due to surface tension. **Figure 36** shows how adding too much solution to a sample will cause it to overflow. Thus, in the end enough solution was needed to cover the sample without causing the surface tension to break.

Figure 37 Dried samples of HAp on Si, ready for scrapping and sintering.

The smallest pipette in our lab was used to dispense the solution. This particular pipette was normally used to clean our DLS machine. This pipette was advantageous for two reasons: it created the smallest droplets, and consistently created ~13 μL droplets. This type of consistency can be seen above in **Figure 37**. Most of the droplets shown are very close in size and shape.

Drying time was also found experimentally. For small amounts of samples, 1 to 10, drying was found to take 20 to 30 minutes to dry. Larger sample batches, such as those in **Figure 37**, could take hours to dry.

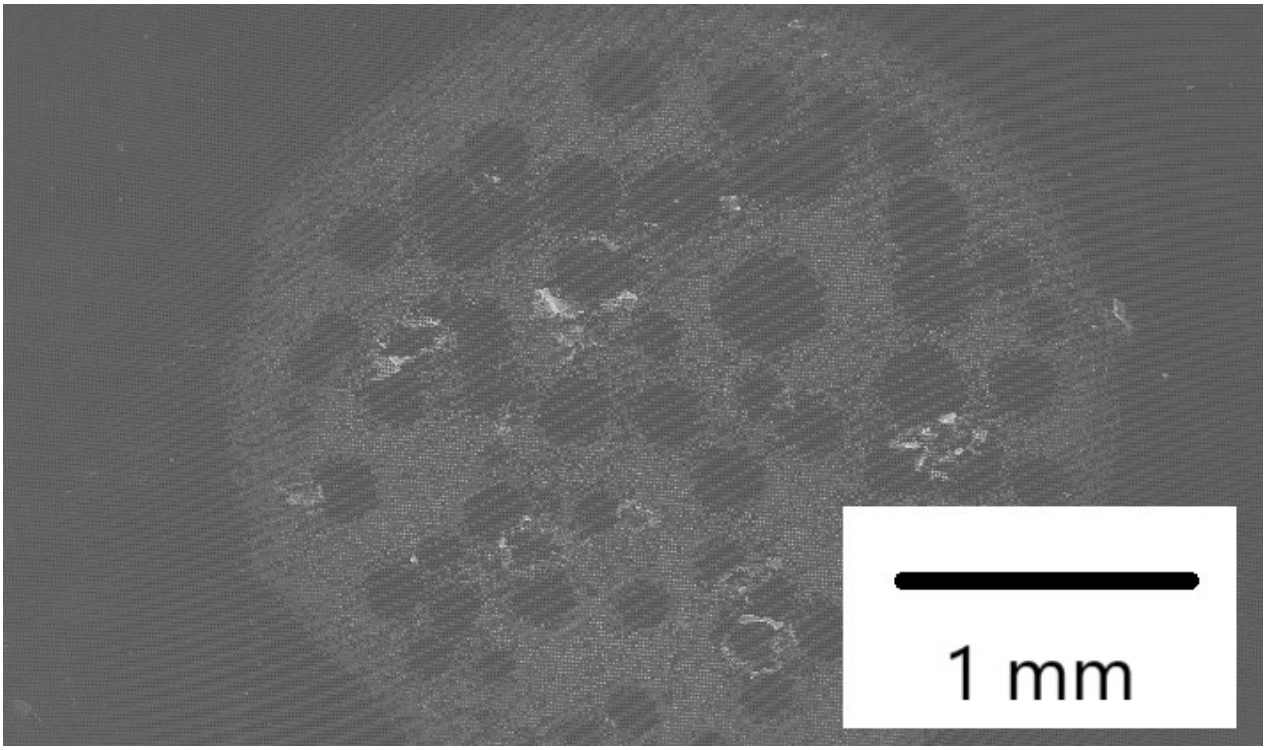

Figure 38 Far shot image of a sintered sample before scrapping.

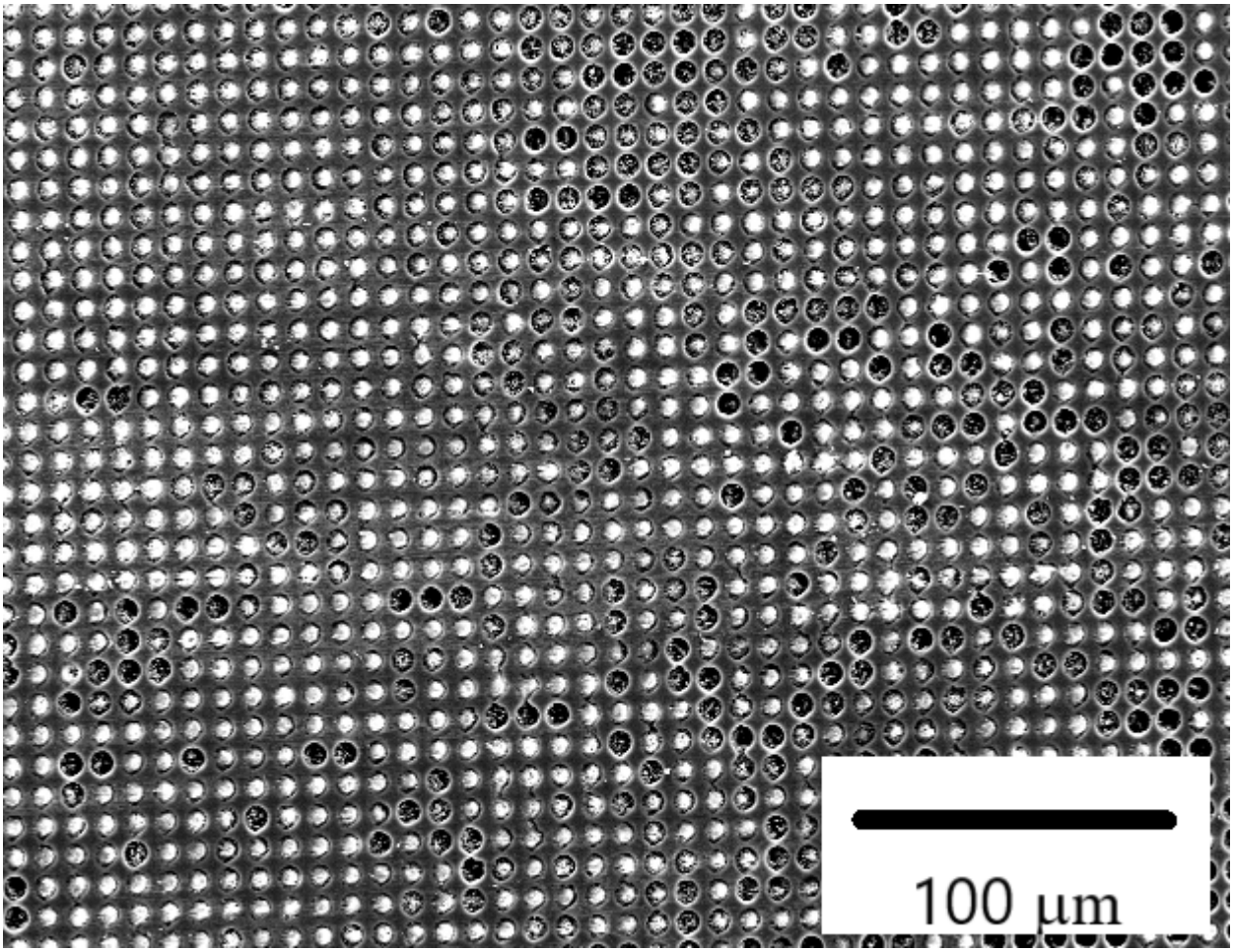

Figure 39 Medium range SEM of a dried HAp sample before scraping and sintering.

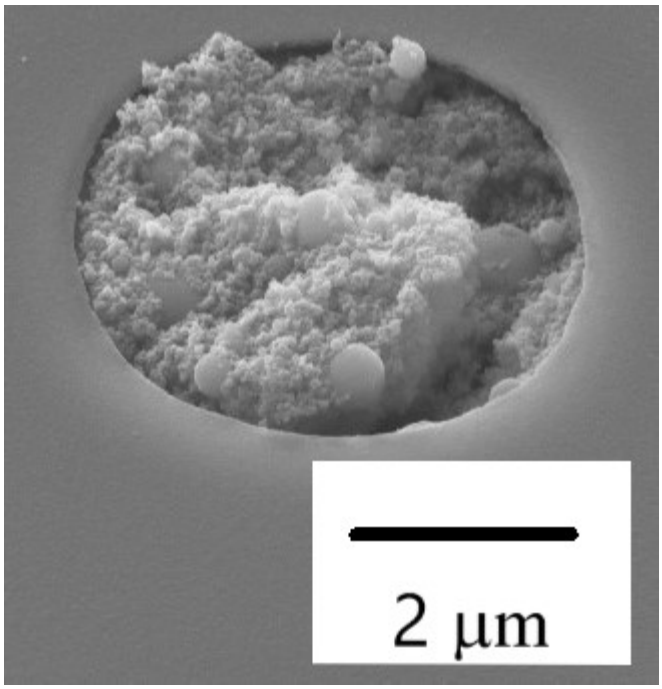

Figure 40 SEM of fully filled cavities.

From **Figure 38 to 40**, they show increasingly microscopic views of the filled cavities and give a better idea of how the cavities are filled. Starting with **Figure 38**, the outline of the solution droplet can be seen with white dried HAp through much of the circle. Bare areas show places where solution was pulled away from some regions. This was seen in some samples if there was less sediment in the solution than others. Typically, droplets that had more ceramics in it filled larger percentages of the circles. If the ceramics were under a certain percentage than these bare areas formed. This slight issue was partially fixed by making sure that when a pipette was filled with the solution, the solution was filled from the bottom of the mixing dish to the point where the pipette would physically touch the bottom. This maximized the amount of ceramics and minimized bare areas that formed.

Figure 39 is an example of what happens when the solution is improved, and there is a more even spread of filled cavities. Although even here there are still unfilled and partially filled

cavities. Several different methods were tried to improve this filling rate even further. One of them was sintering specimens repeatedly and filling the cavities with more slurry between each sintering session. However, this method ran an issue of formation of oxides on the silicon substrate in the form of silicon dioxide and chrome oxides of some variety after sintering. Oxides in general are highly hydrophilic, so when droplets were placed in the sample, the solution spread over the entire surface and started forming films instead of filling the cavities. Another method to avoid partially filled cavities was reapplying solutions of HAp after the initial drying; this procedure was repeated up to four times. Although hypothetically this would help to fill more cavities and have a generally better filled sample, no major visible differences were seen when comparing samples that had been filled four times versus once.

While **Figure 39** shows an above view with numerous cavities, this perspective does not give the best view to tell if cavities have been filled well enough. However, this figure does show a general pattern of whether or not cavities are filling. **Figures 40 (a) and (b)** show a close view

of completely filled and almost filled cavities. The powders settled well into each cavity and there was no outward sign of agglomeration.

3.3 Sintering Samples

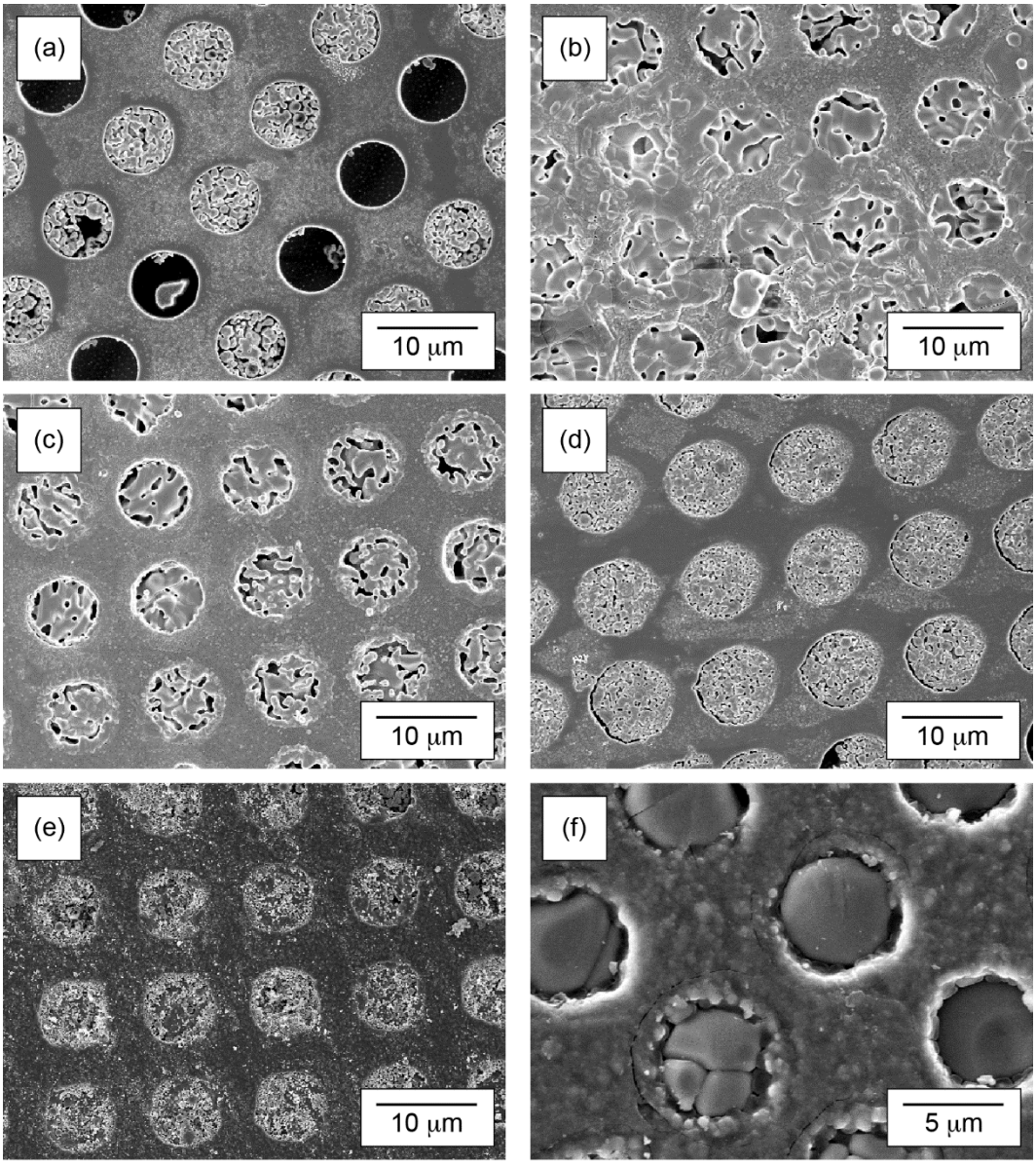

Figure 41 Sintered Samples at (a) 700°C, (b) 800°C, (c) 900°C, (d) 1000°C, (e) 1100°C, and (f) 1250°C.

According to the previous studies by Ramesh *et al*. [Ramesh_2000, 2011, 2012], commercially produced HAp powders need to be sintered at temperatures of at least 1200°C in order to sinter full density. Ramesh *et al*. also showed that starting around 1300°C both fracture toughness and Vickers hardness of HAp begin to drop. In addition, experiments conducted by Thangamani *et al.* [101] studied the effects of powder processing on densification, microstructure

and mechanical properties of HAp. It was verified that samples reached maximum sintering density and hardness between 1200°C and 1300°C. In general, most publications on this subject support the claim that maximum density and hardness for HAp materials is found between 1200°C and 1300°C, including articles by Prokopiev and Sevostianov [102] and Georgiou *et al*. [103]. Sintering beyond this temperature range begins to decompose the HAp, as well as weaken its density and hardness. Thus, we chose 1250°C for maximum sintering temperature as an intermediary between 1200°C and 1300°C.

Figure 41 shows that the density of the sintered powders increased with temperature from 700°C to 1250°C. From **Figure 41(f)**, the top surface of samples can vary [104], since the top of the molds are not covered. This variety in surface and shape is due to uneven filling from cavity to cavity, and shrinking during sintering.

Sintering beyond 1300°C could also cause the decomposition of HAp into tricalcium phosphate (TCP) and tetracalcium phosphate (TTCP). TTCP is only formed at high temperatures above 1300°C [105]. Numerous sintering temperatures between 700°C and 1250°C were tested to find what temperature would produce the densest samples. Theoretically as stated by Ramesh, Prokopiev, Ruys, Zhang, and Pramanik, the optimum sintering temperature for conventional furnace sintering is between 1200°C and 1300°C. **Figure 41** shows clearly that the density of the sintered specimens increases with temperature from 700°C to 1250°C. Our results agreed with

Ramesh's results from 2000, 2011, and 2012, that 1250°C produces the densest HAp samples.

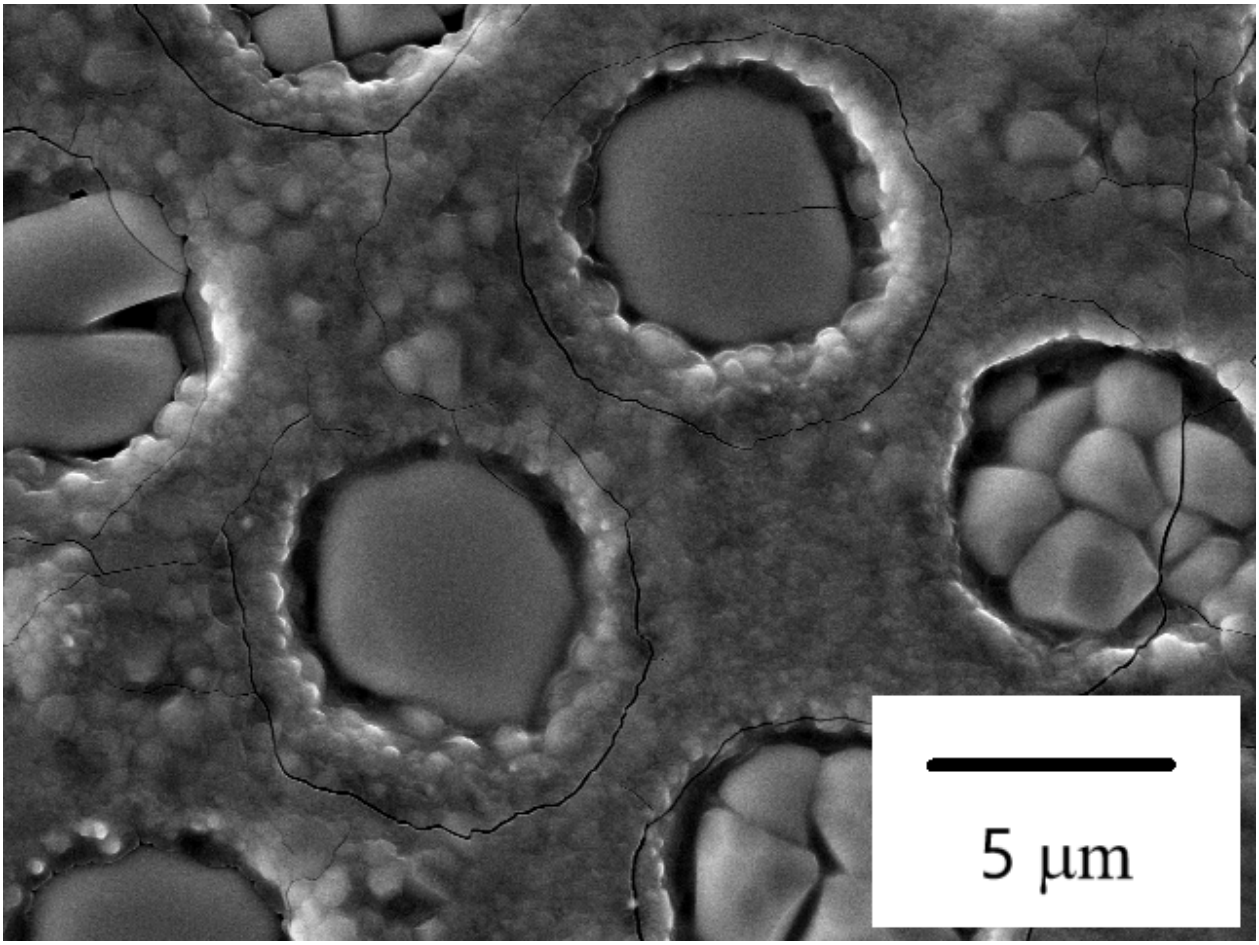

Figure 42 SEM of sintered HAp in cavities.

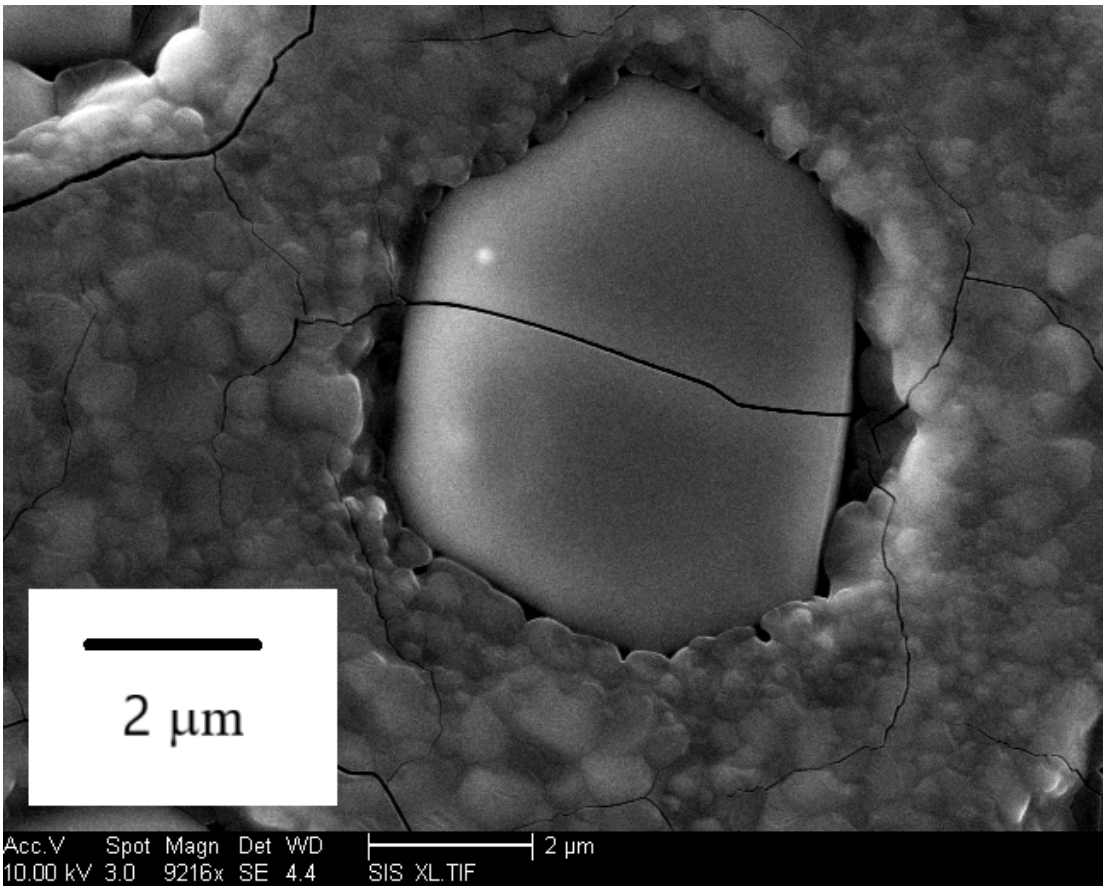

Figure 43 SEM close-up of a post sintered HAp in cavity.

Upon closer examination of **Figures 42** and **43** it is clear to see that the samples were fully sintered and reached a high degree of density. However, there is evidence of cracking in most samples (see **Figure 42**). This can be attributed to thermal stress cracking from heating or cooling too quickly. In research by Oleg Prokopiev *et al*. different sintering methods of HAp were discussed and researched to understand the dependence of the mechanical properties of HAp on the sintering temperature. They found that although furnace sintering is the most common due to its simplicity, it has a major flaw in that this method generates thermal and residual stress fields

due to the low heat conductivity and shrinkage of HAp. This in turns leads to the formation of small cracks in the sample. They stated that to avoid this, the ramping temperature should not exceed 5°C/min, although this will fluctuate depending on the sample size. The larger the sample the lower the rate needs to be. The images of our sintered specimens (see **Figures 42** and **43**) show that the heating rate we used (5°C/min) was still too high to eliminate these thermal stresses. Theoretically, a lower heating rate would reduce or remove these defects. Rates closer to 2°C or 3°C/min would have been preferred, as used in research by Pramanik and Prokopiev, who used rates of 200°C/hr (3.33°C/min) and 1°C/min respectively. These incredibly low ramping rates that lead up to high temperatures do mean that this method is incredibly time and energy consuming, but it does allow for a wide range of sizes and shapes of materials to be sintered without cracking. Thus, it is possible to eventually sinter a whole wafer, rather than just small pieces of it, due to the large chambers in the furnace.

3.4 Removal of Samples from Cavities

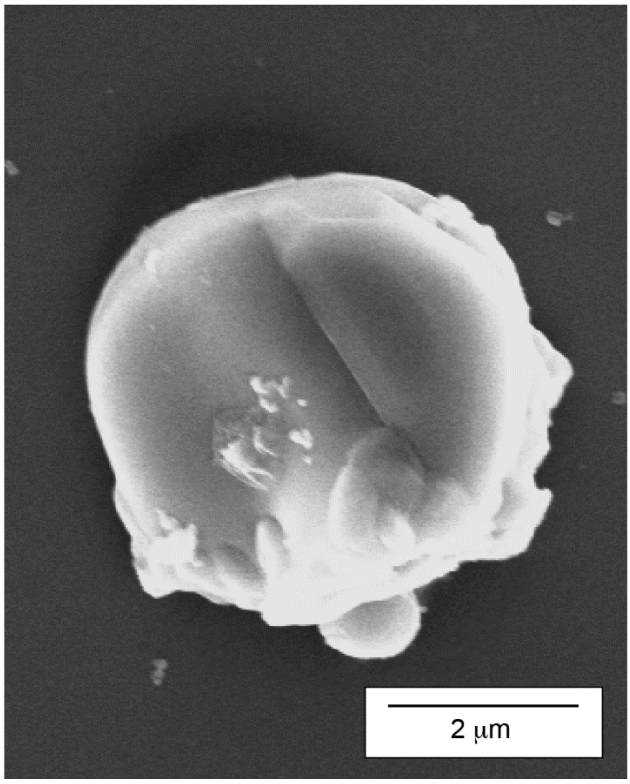

Figure 44 Close-up view of ejected cylinders sintered at 1250°C.

It was found that sintered samples could be ejected from molds by placing them upside down in a liquid solution and ultrasonicating for a short time. The samples came out easily because cylinders shrink away from the edges of the sample during the sintering process, minimizing surface contact. However, overall the powders resemble the mold they were cast in (**Figure 44**). **Figure 44** shows a released sample fully sintered at 1250°C. The sintered samples were close to the desired 5 × 5 μm dimensions. A general cylindrical shape is also seen here, with a few macroscopic defects attached to the side and the top of the sample. Cracks formed in some of the cylinders, as seen in **Figure 43(f)**, but this was expected since our heating and cooling rates could not be as finely controlled as those performed by Ramesh *et al*. [Ramesh_2000, 2011, 2012] or

Grossenchaber *et al*. [106].They used rates of 2°C/min and ~0.167°C/min respectively, while ours was 5°C/min.

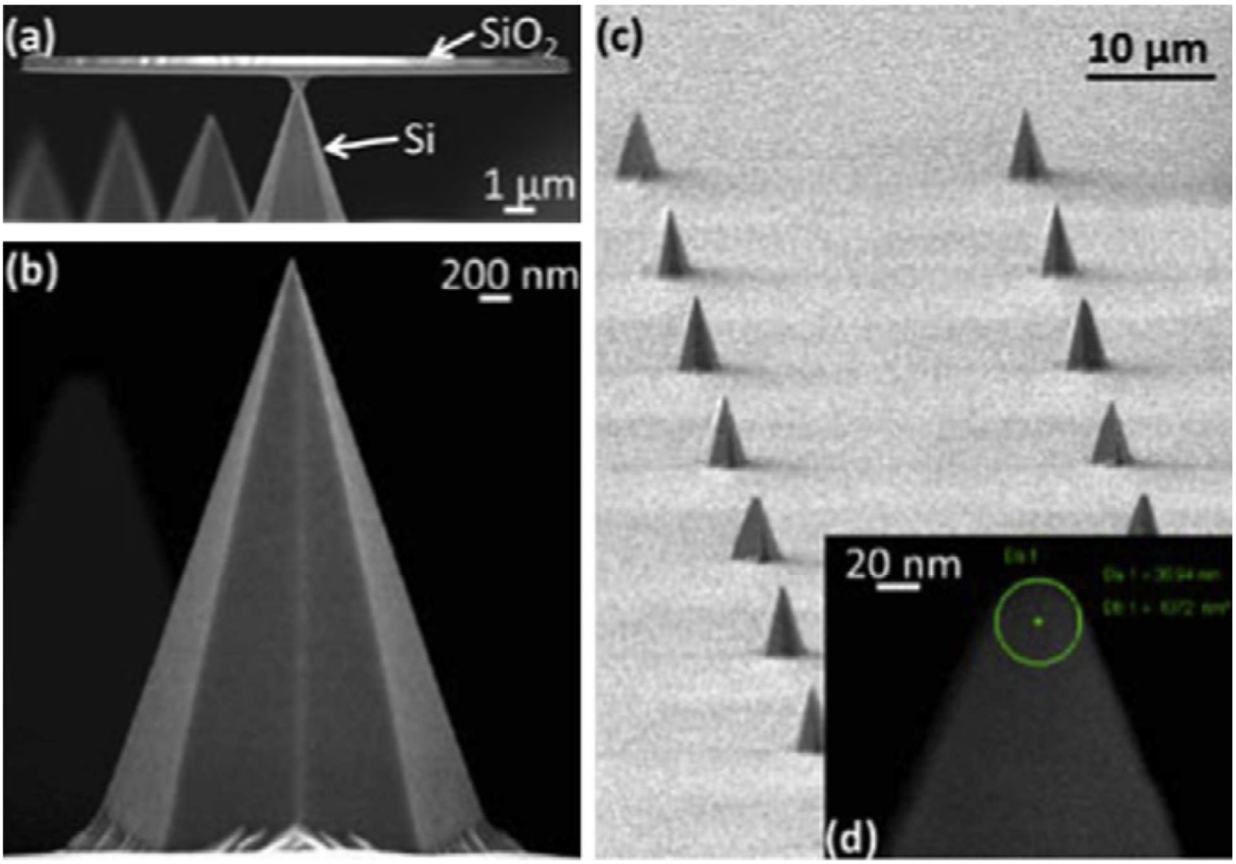

Figure 45 SEM images of nano-tipped SiCO needles (reprinted with permission)[109].

Grossenbacher was able to create nanometer tipped cones of ~12µm in height made up of Silicon Carbide. These nanometer tipped cones appeared free of cracks. This can be attributed to the low heating and cooling rates [107]. Lowering the heating and cooling rates is an area that requires further investigation. If successful it could improve the quality of the resultant materials.

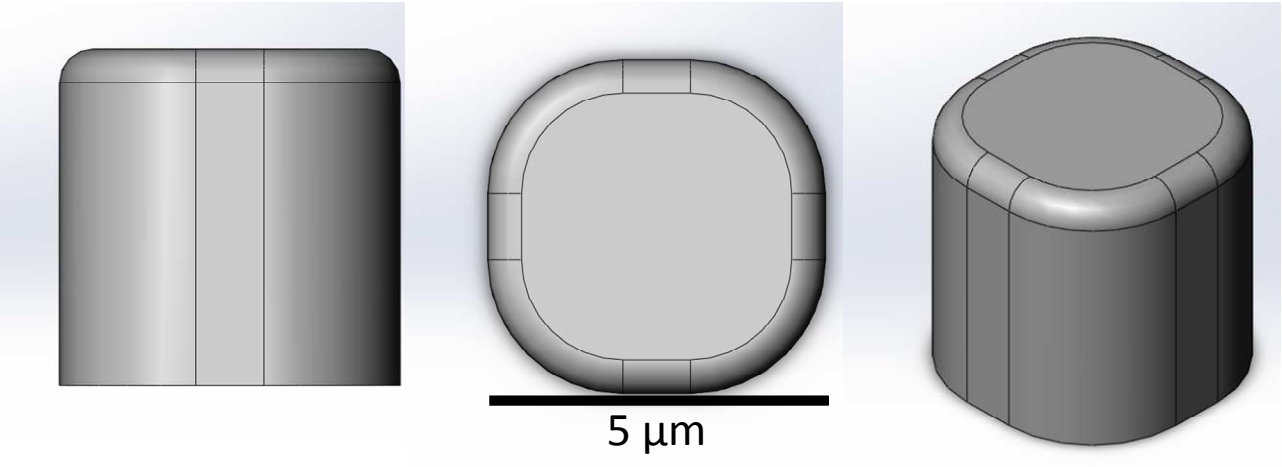

Figure 46 Models of hypothetically what HAp structures would look like when removed from silicon substrate, produced using Solidworks. **(a)** Side view, **(b)** top view, **(c)** corner view, dimensions are 5 µm in height and 5 µm in diameter.

Figures 46 show what the hydroxyapatite would hypothetically look like if it was shaped exactly like the mold it was caste in. We strive to get as close as we can to the exact model.

Theoretically, the shapes of the HAp would resemble 5 µm cubes that have 1 µm radius rounded corners, similar to what is shown in **Figure 46**. This assumes little to no malformations due to shrinkage during sintering or other debris or possible agglomerations. The top is shown to be rounded. This is due to the assumption that during sintering the HAp sample will shrink. However, the top could end up flat if there was minimal shrinkage, or if there was enough leftover material on the top to allow for a more flat surface to form.

Figure 46 demonstrates that the edges of the samples were planned to be smooth, due to the smoothness of the cavities. This smoothness was planned for the sides and bottom of samples. It can also be seen that heights were assumed to reach 5 µm, since this was the height of the cavity.

However if the cavity was not able to be filled all the way to the top or if there was excessive material, it was possible for the height to be slightly above or below 5 µm.

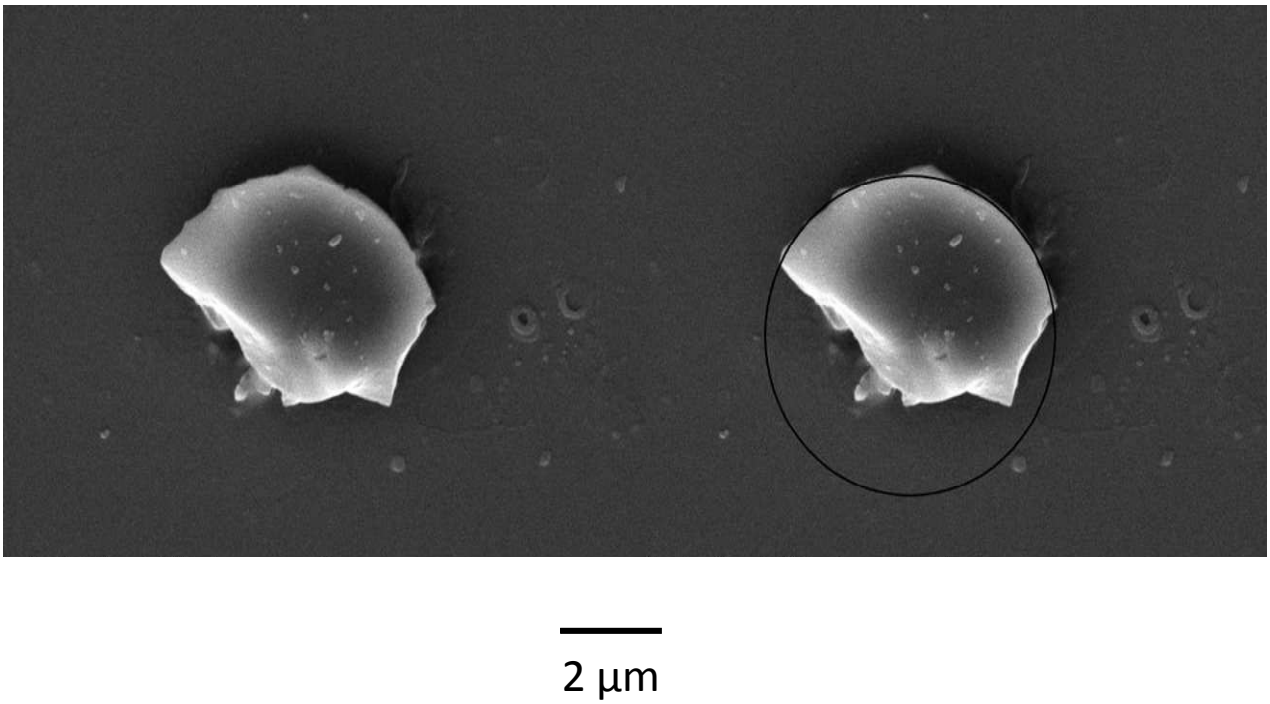

Figure 47 SEM comparison of **(a)** original image, **(b)** original shape if together.

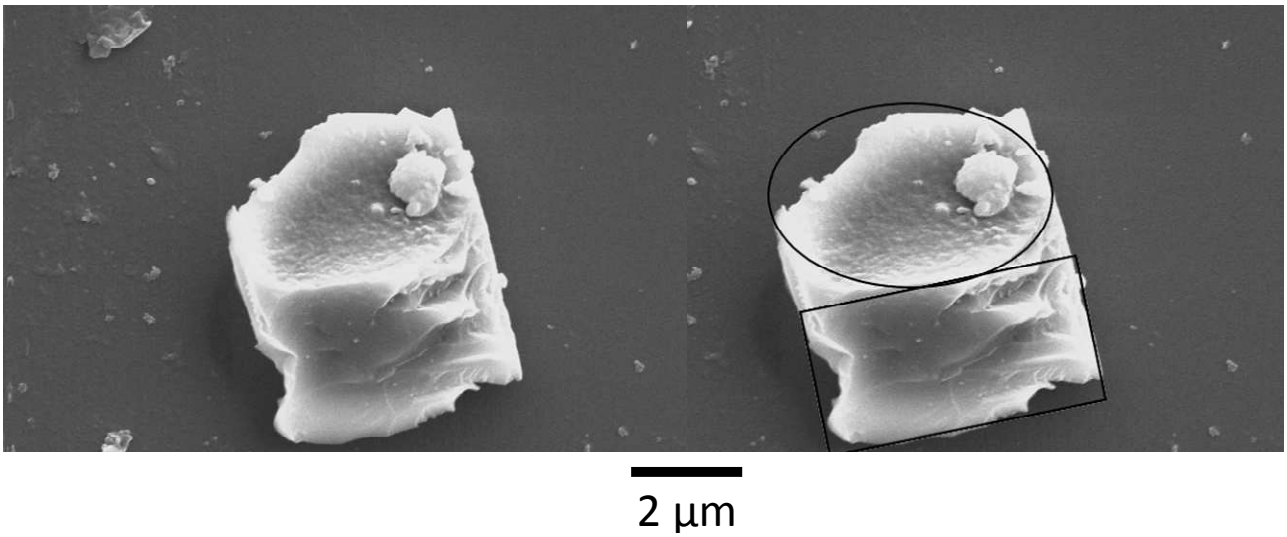

Figure 48 SEM comparison of **(a)** original image, **(b)** original shape if together.

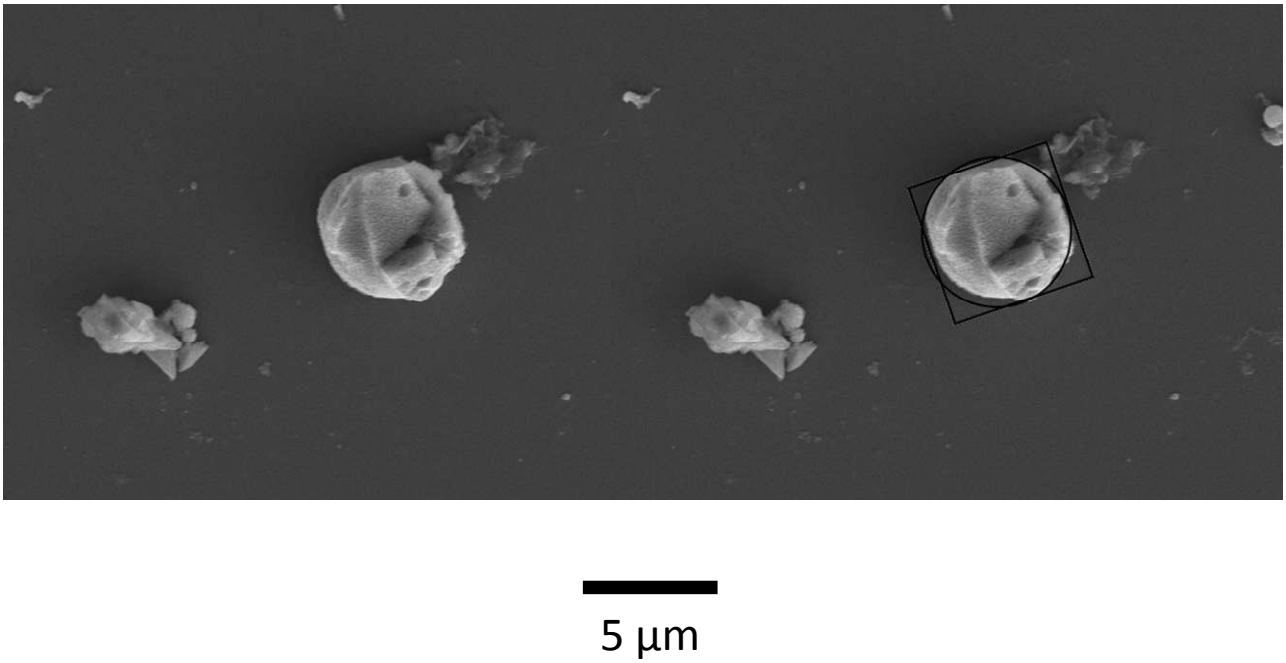

Figure 49 SEM comparison image **(a)** unchanged**, (b)** with changes.

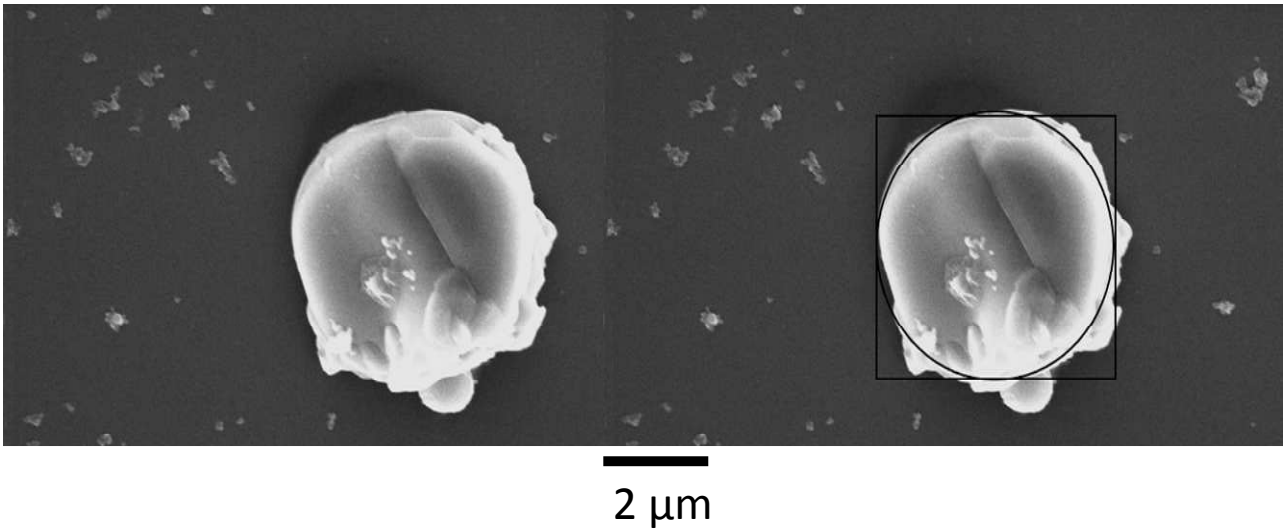

Figure 50 SEM comparison of **(a)** original image, **(b)** if original shape.

Upon analyzation of the extracted samples it was found that the samples did resemble the cavities they were caste in, although not exactly as planned, or shown in **Figures 47-50**. Some shapes more closely resembled the mold than others. This is due to the fact that our process is not able to finely control how much material is placed in each cavity, as well as the heating and cooling rates.

These cracks caused the samples to break apart upon removal. However, as more and more samples were viewed it was found that these broken pieces were indeed molded samples due to their distinct appearance from background material that had been removed as well. This distinct appearance came in the form of a brighter white color as well as having a visible shape that appeared controlled rather than random.

When looking at **Figures 47-50** one can see an unaltered image on the left that shows a view of the broken pieces of samples. This is most evident in **Figure 47** where approximately only

one third of the sample can be seen. The breaks along the bottom of the sample show clear cracks from the whole piece. The piece was found to be a proper molded sample, because of the clean breaks from it, smooth looking top, correct size, and general circular like geometric shape. When the outline of a circle is placed overlapping an image of the sample it lines up incredibly well with it. This further proves that this broken piece was indeed a complete sample before the removal. This particular figure is meant to be an evidence that although not all samples stayed together after removal, upon closer examination and review pieces of these samples can be found and shown to have geometric shapes and sizes that are consistent with what molds they were caste in.

Figures 48, 49 and **50** are different from **47** in that they are not missing as much of their complete sample. **Figure 48** is a great example showing a more definite square like appearance to the sample than the normal cylindrical or cylindrical cube shape. It is indeed a removed sample because it has the correct dimensions, color appearance, and general shape that was desired. The sample is a little shorter than 5 μm, but this can be attributed to the cavity not filling completely, as seen in previous sections.

Figures 49 and **50** show samples that are the closest resemblance to the molds that were found. As stated previously, the shapes should hypothetically have roughly 3μm long edges with curved edges that were about 1 μm. Upon closer examination the samples shown in these two figures are quite close to these dimensions. The smooth, straight edges are visible and the slightly rounded corners are also obvious. Although the dimensions of the edges and corners are not exactly to specification, they are within reason. Since there are numerous factors that can influence the end size of the sample it is acceptable to have dimensions that are slightly smaller than planned. Smaller sizes can be attributed to shrinkage during the sintering process. Larger sizes, although not impossible, are highly unlikely due to the homogeneity of the molds. However, there is a

possibility for molds to vary slightly due to defects during the processing work, thus creating cavities that are larger than expected.

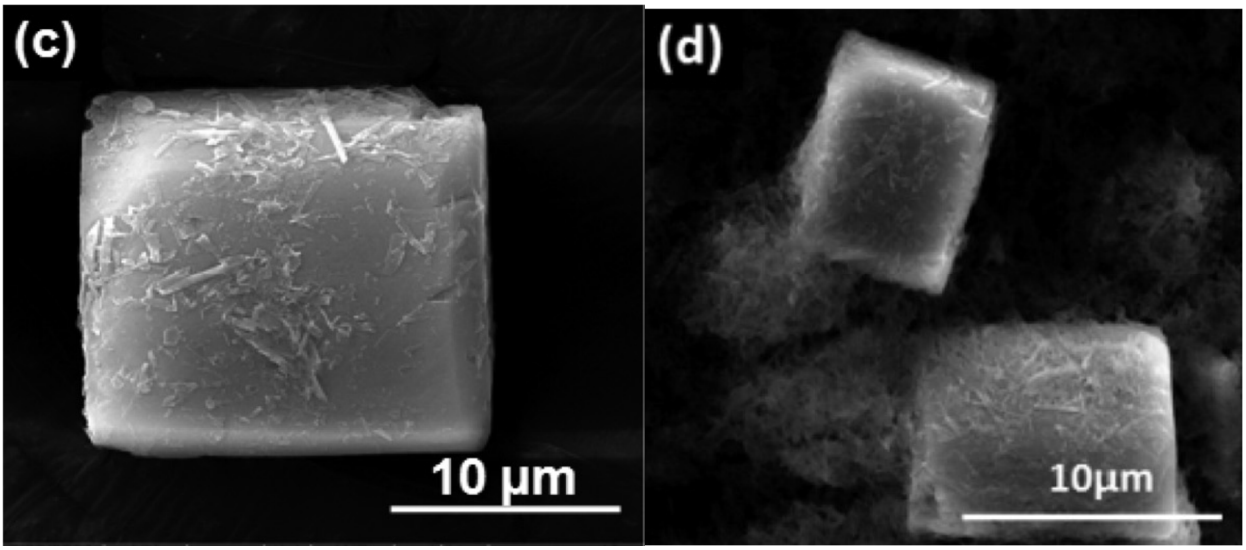

Figure 51 SEM of controlling powder to form cubes using hydrothermal synthesis (reprinted with permission) [28].

When comparing the extracted samples to the HAp cubes that were grown by I. Mary and her team there are many major differences as well as some similarities. Her team was able to create cubic structures of HAp at the micrometer scale, which is what this project had tried to pursue at the beginning. Initially this method of using hydrothermal processing was appealing, however due to equipment difficulties it was abandoned. The method was appealing due to the ability to create micrometer scale cubes of HAp. However controlling the size would require experiments as those created by Mary and her team varied in size. As seen above in **Figure 51**, some cubes are close to 20 µm while others were 10 µm or less in some cases. Thus, despite the ability to create really accurate and good-looking cubes at the proper scale there is an issue of homogeneity which would need to be addressed. Hypothetically this could be addressed by experimenting with variables of the experiment, but we did not have access to a working autoclave so this would not work. Despite

this, the work done by Mary and her team show that cubes are indeed possible to create at the micrometer scale.

Once the HAp samples have been removed from the cavities the question of can the molds be reused arises? This would save a lot of time and money by not having to continuously create new molds to sinter new cylinders. The process to achieve this was somewhat researched and tested. It was found that to achieve the recycling of the molds, the Cr mask would need to be removed before filling the cavities with slurry. This is done by placing the wafer sample into a wet Cr etching solution that will eat away the Cr, but not the silicon. This is important because to reuse the wafer, the sample would need to be placed in HF or in an HF buffer solution. This would remove all silicon oxides from the surface as well as the HAp, thus cleaning the surface and removing the hydrophilic nature of the surface. It was found that if this removal in HF is tried while there is still a layer of Cr, then the HF dip does not work because HF does not erode Cr. Thus, the necessity to remove the Cr mask after etching has been completed. If that is done, then once HAp samples have been removed from the cavities then it is hypothetically an easy process to clean the wafers. Theoretically the HF or HF buffer solution would quickly remove all silicon oxides from the surface as well as leftover HAp. Then the wafer would need to be cleaned in water, and dried before being used again. This was not tested first hand, due to constraints of the project, but after considerable talk with those in the Nano3 lab and related fields, this process was found to be quite plausible and promising.

In summary, our work explored the innovative technique of controlling morphology of HAp by using molding and casting techniques. Fully dense cylindrically shaped samples produced from a slurry of DI water, HAp powder, and Darvan 811 dispersant, were formed by

sintering at 1250°C. Sintered samples resembled the cylindrical molds in which they were cast in. This research took a fresh look at another way to control morphology of ceramic materials.

4. Conclusion

A novel approach to ceramic morphology control was demonstrated by using micrometer scale molding and casting to control the morphology of sintered cylinders of hydroxyapatite. In particular, a process that created 5 μm × 5 μm cylindrical cavities into a 500 μm thick silicon wafer was developed. The process consisted of reactive ion etching, in particular the silicon waveguide method. Silicon waveguide produced smooth walls, thus no further etching was required. HAp slurry was made by combining deionized water, HAp powder, and Darvan 811 dispersant. The dispersant was necessary to prevent agglomeration before sintering and to produce denser final product. Highly dense samples were formed after sintering at 1250°C with sintered specimens being extracted as cylinders. The success here paves the way to improve the process of creating higher yield batches of cylindrically-shaped ceramic samples that are micrometer in size. With refinement, this approach would allow for large numbers of similar micrometer-scaled specimens to be created. In addition, different shapes such as cones, cubes, and hexagons, could potentially be produced by this method.

5. References

[1] Hydroxyapatite Model. http://www.chemtube3d.com/images/craigimages/CraigMichael/i624fg51.png

[2] M. Markovic, B.O. Fowler, M.S. Tung, Preparation and Comprehensive Characterization of a Calcium Hydroxyapatite Reference Material, Journal of Research of the National Institute of Standards and Technology, 109 (2004) 553-568

[3] V.S. Kattimani, S. Kondaka, K.P. Lingamaneni. Hydroxyapatite – Past, Present, and Future in Bone Regeneration, Bone and Tissue Regeneration Insights, **7** (2016) 9-19

[4] Diagram of the inside of a human bone. https://www.google.com/imgres?imgurl=http%3A%2F%2Fwww.mhhe.com%2Fbiosci%2Fap%2Fap_casestudies%2Fimages%2Ffig15.gif&imgrefurl=http%3A%2F%2Fwww.mhhe.com%2Fbiosci%2Fap%2Fap_casestudies%2Fcases%2Fanswers%2Fap-answer_case06-04.html&docid=xpgYflxiAjuBvM&tbnid

[5] C.J. Damien, J.R. Parsons, Bone Graft and Bone Graft Substititutes: A Review of Current Technology and Applications, Applied Biomaterials, 2:3 (1991) 187-208

[6] Diagram of a tooth. https://pocketdentistry.com/wp-content/uploads/285/c05f0011.gif

[7] J.L. Ong, D.C.N. Chan, Hydroxyapatite and Their use As Coatings in Dental Implants: A Review, Critical Reviews in Biomedical Engineering, 25(5&6) (1999) 667-707

[8] E.I. Shishatskaya, I.A. Hlusov, T.G. Volova, "A hybrid PHB-hydroxyapatite composite for biomedical application: production, in vitro and in vivo investigation", Journal of Biomaterials Science, Polymer Edition, 17:5 (2006) 481-498

[9] Campbell Allison, Bioceramics for implant coating, MaterialsToday, 6(11) (2003) 26-30

[10] Wojciech Suchanek, Masahiro Yoshimura, Processing and properties of hydroxyapatite-based biomaterials for use as hard tissue replacement implants, Journal of Materials Research, 13(1) (1997) 94-117

[11] Jean-Alain Epinette. Long lasting outcome of hydroxyapatite-coated implants in primary knee arthroplasty: a continuous series of two hundred and seventy total knee arthroplasties at fifteen to twenty two years of clinical follow-up, International Orthopaedics, 38(2) (2014) 305-311

[12] Sandra Franz, Stefan Rammelt, Dieter Scharnweber, Jan C. Simon, Immune responses to implants – A review of the implications for the design of immunomodulatory biomaterials, Biomaterials, 28, (2011) 6692-6709

[13] Alis Yovana Pataquiva-Mateus, Maria Pia Ferraz, Fernando Jorge Monteiro, Nanoparticles of hydroxyapatite: preparation, characterization and cellular approach – An

Overview, MUTIS, Journal of the Faculty of Sciences and Engineering, 3(2) (2013) 43-57

[14] M. Navarro, A. Michiardi, O. Castano and J. A. Planell, Biomaterials in orthopaedics, Journal of the Royal Society Interface, 5(27) (2008) 1137-1158

[15] Irena Gotman, Characteristics of Metals Used in Implants, Journal of Endourology, 11(6) (1997) 382-389

[16] AFM and SEM Imaging of Bone. http://hansmalab.physics.ucsb.edu/afmbone.html

[17] Jean-Alain Epinette, Long lasting outcome of hydroxyapatite-coated implants in primary knee arthroplasty: a continuous series of two hundred and seventy total knee arthroplasties at fifteen to twenty two years of clinical follow-up, International Orthopaedics, 68A, Issue I (2014) 123-132

[18] C.E. Wilson, J.D. de Bruijin, C.A. van Blitterswijk, A.J. Verbout, W. J. A. Dhert, Design and fabrication of standardized hydroxyapatite scaffolds with a defined macro-architecture by rapid prototyping for bone-tissue-engineering research, Journal of Biomedical Materials Research, 68(1) (2004) 123-132

[19] Sylvain Deville, Eduardo Saiz, Antoni P. Tomsia, Freeze casting of hydroxyapaptite scaffolds for bone tissue engineering, Biomaterials, 32 (2006) 5480-5489

[20] Hassna Rehman Ramay, Miqin Zhang, Preparation of porous hydroxyapatite scaffolds by combination of the gel-casting and polymer sponge methods, Biomaterials, 24(19) (2003) 3293-3302

[21] Barbara Leukers, Hulya Gulkan, Stephan H. Irsen, Stefan Milz, Carsten Tille, Matthias Schieker, Hermann Seitz, Hydroxyapatite scaffolds for bone tissue engineering made by 3D printing, Journal of Materials Science: Materials in Medicine, 16(12) (2005) 1121-1124

[22] T.H. Ang, F.S.A Sultana, D.W. Hutmacher, Y.S. Wong, J.Y.H. Fuh, X.M. Mo, H.T. Loh, E. Burdet, S.H. Teoh, Fabrication of 3D chitosan – hydroxyapatite scaffolds using a robotic dispensing system, Materials Science and Engineering, 20(1-2) (2002) 35-42

[23] Aziz Fihri, Chrtophe Len, Rajender S. Varma, Abderrahim Solhy, Hydroxyapatite: A review of syntheses, structure and applications in heterogeneous catalysts, Coordination Chemistry Reviews, 347 (2017) 48-76

[24] I. Sopyan, E. Pusparini, S. Ramesh, C.Y. Tan, Y.C. Ching, Y.H. Wong, N.I. Zainal Abidin, Hari Chandran, S. Ramesh, L.T. Bang, Influence of sodium on the properties of sol-gel derived hydroxyapatite powder and porous scaffolds, Ceramics International, 43(15) (2017) 12263-12269

[25] Luz. A. Zavala-Sanchez, G.A. Hirata, E. Novitskaya, K. Karandikar, M. Herrera, O.A. Graeve, Distribution of Eu2+ and Eu3+Ions in Hydroxyapatite: A Cathodoluminescence and Raman Study, ACS Biomaterials Science and Engineering, 1(12) (2015) 1306-1313

[26] M.R. Saeri, A. Afshar, M. Ghorbani, N. Ehsani, C.C. Sorrell, The wet precipitation process of hydroxyapatite, Materials Letters, 57(24-25) (2003) 4064-4069

[27] B. Nasiri-Tabrizi, P. Honarmandi, R. Ebrahimi-Kahrizsangi, P. Honarmandi, Synthesis of nanosize single-crystal hydroxyapatite via mechanochemical method, Materials Letters, 63(5) (2008) 543-546

[28] I. Reeta Mary, S. Sonia, S. Viji, D. Mangalaraj, C. Viswanathan, N. Ponpandian, Novel multiform morphologies of hydroxyapatite: Synthesis and growth mechanism, Applied Surface Science, 361 (2015) 25-32

[29] Diagram of Sol-gel synthesis. https://en.wikipedia.org/wiki/Sol-gel .

[30] G. Bezzi, G. Celotti, E. Landi, T.M.G. La Torretta, I. Sopyan, A. Tampieri, A novel sol-gel technique for hydroxyapatite preparation, Materials Chemistry and Physics, 78(3) (2002) 816-824

[31] K.P. Sanosh, Min-Cheol Chu, A. Balakrishnan, Yong-Jin Lee, T.N. Kim, Seong-Jai Cho, Sythesis of nano hydroxyapatite powder that simulate teeth particle morphology and composition, Current Applied Physics, 9(6) (2009) 1459-1462

[32] C. Barry Carter, M. Grant Norton, Sols, Gels, and Organic Chemistry, Ceramic Materials, (2013) 400-411

[33] Kashinath C Patil, Singanahally T Aruna, and Sambandan Ekambaram, Combustion Synthesis, Current Opinion in Solid State & Materials Science, 2(2) (1997) 158-165

[34] Singanahally T. Aruna, Alexander S. Mukasyan, Combustion synthesis and nanomaterials, Current Opinion in Solid State and Materials Science, 12 (2008) 44-50

[35] Kenneth M. Harris, Mechanochemical synthesis: How grinding evolves, Nature Chemistry, 5 (2012) 12-14

[36] Carolina Mochales, Hassane El Briak-BenAbdeslam, Maria Pau Ginebra, Alain Terol, Josep A. Planell, Philippe Boudeville, Dry Mechanochemical synthesis of hydroxyapatites form DCPD and CaO: influence of instrumental parameters on the reaction kinetics, Biomaterials, 7-8 (2003) 1151-1158

[37] Abbas Fahami, Reza Ebrahimi-Kahrizsangi, Bahan Nasiri-Tabrizi, Mechanochemical synthesis of hydroxyapatite/titanium nanocomposite, Solid State Sciences, 13(1) (2010) 134-141

[38] Hao Wu, Qiang Li, Application of Mechanochemical synthesis of advanced materials, Journal of Advanced Ceramics, 1(2) (2011) 130-137

[39] Diagram of an autoclave. http://pubs.rsc.org/services/images/RSCpubs.ePlatform.Service.FreeContent.ImageService.svc/ImageService/Articleimage/2014/CS/c3cs60219b/c3cs60219b-f3_hi-res.gif

[40] Ines S. Neira, Yury V. Kolen'ko, Oleg I. Lebedev, Gustaaf Van Tendeloo, Himadri S. Gupta, Francisco Guitian, and Masahiro Yoshimura, An Effective Morphology Control of Hydroxyapatite Crystals via Hydrothermal Synthesis, Crystal Growth and Design, 9(1) (2008) 466-474

[41] Rodica-Mariana Ion. Hybrid composite materials with biofunctional properties, Journal of Optoelectronics and Advanced Materials, 15 (7-8) (2013) 874-878

[42] Peipei Wang, Caihong Li, Haiyan Gong, Xuerong Jiang, Hongqiang Wang, Kaixing Li, Effects of synthesis conditions on the morphology of hydroxyapatite nanoparticles produced by wet chemical process, Powder Technology, 203(2) (2010) 315-321

[43] Naruporn Monmaturapoj, Nano-size Hydroxyapatite Powders Prearation by Wet-Chemical Precipitation Route, Journal of Metals, Materials and Minerals, 18(1) (2008) 15-20

[44] M.R. Saeri, A. Afshar, M. Ghorbani, N. Ehsani, C.C. Sorrell, , The wet precipitation process of hydroxyapatite, Materials Letters, 57 (2003) 24-25

[45] Y.X. Pang, X. Bao, Influence of temperature, ripening time and calcination on the morphology and crystallinity of hydroxyapatite nanoparticles, Journal of the European Ceramic Society, 23(10) (2002) 1697-1704

[46] Cox Sophie, Synthesis Method of Hydroxyapatite, ResearchGate, (2015)

[47] Nayak Amit, Hydroxyapatite Synthesis Methodologies: An Overview, International Journal of ChemTech Research, 2(2) (2010) 903-907

[48] D. Gopi, L. Kavitha, D. Rajeswari, Synthesis of Pure and Substituted Hydroxyapatite Nanoparticles by Cost Effective Facile Methods, Handbook of Nanoparticles, (2015) 167-190

[49] Pierre Layrolle, Atsuo Ito, Tetsuya Tateishi, Sol-Gel Synthesis of Amorphous Calcium Phosphate and Sintering into Microporous Hydroxyapatite Bioceramics, Journal of American Ceramic Society, 81(6) (1998) 1421-1428

[50] A.J. Ruys, C.C. Sorrell, A. Brandwood, B.K. Milthorpe, Hydroxyapatite sintering characteristics: correlation with powder morphology by high-resolution microscopy, Journal of Materials Science Letters, 14 (1995), 744-747

[51] S.J. Kalita, S. Bose, H.L. Hosick, A. Bandyopadhyay, CaO-P2O5-based sintering additives for hydroxyapatite (HAp) ceramics, Biomaterials, 25(12) (2003) 2331-2339

[52] A.J. Ruys, M. Wei, C.C. Sorrell, M.R. Dickson, A. Brandwood, B.K. Milthorpe, Sintering effects on the strength of hydroxyapatite, Biomaterials, 16(5) (1995) 409-415

[53] Nasser Y. Mostafa, Characterization, thermal stability and sintering of hydroxyapatite powders prepared by different routes, Materials Chemistry and Physics, 94(2-3) (2005) 333-341

[54] Sumit Pramanik, Avinash Kumar Agarwal, K.N. Rai, Ashish Garg, Development of high strength hydroxyapatite by solid-state-sintering process, Ceramics International, 33(3) (2005) 419-426

[55] Oleg Prokopiev, Igor Sevostianov, Dependence of the mechanical properties of sintered hydroxyapaptite on the sintering temperature, Materials Science and Engineering, 431(1-2) (2006) 218-227

[56] S. Vijayan, Harikrishna Varma, Microwave sintering of nanosized hydroxyapatite powder compants, Materials Letters, 56(5) (2001) 827-831

[57] Yunzhi Peter Yang, Joo L Ong, Jiemo Tian, Rapid sintering of hydroxyapatite by microwave processing, Journal of Materials Science Letters, 21 (2002) 67-69

[58] Yi Fang, Dinesh K. Agrawal, Della M. Roy, Rustum Roy, Microwave sintering of hydroxyapatite ceramics, Materials Research Society, 9(1) (1994) 180-187

[59] Abhijit Chanda, Sudip Dasgupta, Susmita Bose, Amit Bandyopadhyay, Microwave sintering of calcium phosphates ceramics, Materials Science and Engineering C, 29(4) (2009) 1144-1149

[60] Abderrahmen Mechay, Hafed El Feki, Frederic Schoenstein, Florent Tetard, Noureddine Jouini, Effect of spark plasma sintering process on the microstructure and mechanical properties of Nano crystalline hydroxyapatite ceramics prepared by hydrolysis in polyol medium, International Journal of Advanced Chemistry, 2(2) (2014) 80-84

[61] Mats Nygren, Zhijian Shen, On the preparation of bio-, nano- and structural ceramics and composites by spark plasma sintering, Solid State Sciences, 5(1) (2002) 125-131

[62] Faming Zhang, Kaili Lin, Jiang Chang, Jianxi Lu, Congqin Ning, Spark plasma sintering of macroporous calcium phosphate scaffolds from nanocrystalline powders, Journal of the European Ceramic Society, 28(3) (2007) 539-545

[63] Li Zhong, Khor Khiam Aik, Transparent Hydroxyapatite Obtained through Spark Plasma Sintering: Optical and Mechanical Properties, Key Engineering Materials, 631 (2014) 51-56

[64] Y.W. Gu, N.H. Loh, K.A. Khor, S.B. Tor, P. Cheang, Spark plasma sintering of hydroxyapatite powders, Biomaterials, 23(1) (2002) 37-43

[65] Xingyuan Gui, Ping Xiao, Fabrication of Nanostructured Hydroxyapatite via Hydrothermal Synthesis and Spark Plasma Sintering, Journal of American Ceramics Society, 88 (2005) 1026-1029

[66] Mehdi Mazaheri, M. Haghighatzadeh, A.M. Zahedi, S.K. Sadrnezhaad, Effect of novel sintering process on mechanical properties of hydroxyapatite ceramics, Journal of Allows and Compounds, 471(1-2) (2008) 180-184

[67] G. Muralithran, S. Ramesh, The effects of sintering temperature on the properties of hydroxyapatite, Ceramics International, 26(2) (1999), 221-230

[68] Gislâine Bezerra Pinto Ferreira, José Ferreira da Silva Jr, Rubens Maribondo do Nascimento, Uílame Umbelino Gomes, Antonio Eduardo Martinelli. Two-Step Sintering Applied to Ceramics, Sintering of Ceramics - New Emerging Techniques, 19 (2012) 424-439

[69] Kaili Lin, Lei Chen, Jiang Chang, Fabrication of Dense Hydroxyapatite Nanobioceramics with Enhanced Mechanical Properties via Two-Step Sintering Process, International Journal of Applied Ceramic Technology, 9(3) (2011) 479-485

[70] Pei Feng, Man Niu, Changde Gao, Shuping Peng, Cijun Shuai, A novel two-step sintering for nano-hydroxyapatite scaffolds for bone tissue engineering, Scientific Reports, 4(5599) (2014)

[71] N.J. Loh, L. Simao, C.A. Faller, A. De Noni Jr., O.R.K. Montedo, A review of two-step sintering for ceramics, Ceramics International, 42 (11) (2016) 12556-12572

[72] Zhang Xihua, Liu Changxia, Li Musen, Bai Yungqiang, Sun Junlong, Fabrication of hydroxyapatite/diopside/alumina composites by hot-press sintering process, Ceramics International, 35(5) 2009 1969-1973

[73] A. Nakahira, T. Murakami, T. Onoki, T. Hashida, K. Hosoi, Fabrication of Porous Hydroxyapatite Using Hydrothermal hot Pressing and Post-Sintering, Journal of the American Ceramic Society, 88(5) (2005) 1334-1336

[74] N.V. Patrakova, A.S. Lysenkov, A.A. Ashmarin, A.A. Egorov, A. Yu. Fedotov, L.I. Shvorneva, V.S. Komlev, S.M. Barinov, Effect of Hot Pressing Temperature on the Microsctructure and Strength of Hydroxyapatite Ceramic, Inorganic Materials: Applied Research, 4(4) (2013) 362-367

[75] R. Halouani, D. Bernache-Assolant, E. Champion, A. Ababou, Microstructure and related mechanical properties of hot pressed hydroxyapatite ceramics, Journal of Materials Science: Materials in Medicine, 5(8) (1994) 563-568

[76] G. Miranda, A. Araujo, F. Bartolomeu, M. Buciumeanu, O. Varvalho, J.C.M Souza, F.S. Silva, B. Henriques, Design of Ti6Al4V-HA compostes produced by hot pressing for biomedical applications, Materials and Design, 108 (2016) 488-493

[77] A. Rapacz-Kmita, C. Paluszkiewicz, A. Slosarczyk, Z. Paskiewicz, FTIR and XRD investigations on the thermal stability of hydroxyapatite during hot pressing and pressureless sintering processes, Journal of Molecular Structure, 744-747 (2005) 653-656

[78] Diagram of lift-off process. https://en.wikipedia.org/wiki/Lift-off_(microtechnology) .

[79] Barbara Freudig, Stefan Hogekamp, Helmar Schubert, Dispersion of poweders in liquids in a stirred vessel, Chemical Engineering and Processing, 38(4-6) (1999) 525-532

[80] Y.X. Pang, X. Bao, Influence of temperature, ripening time and calcination on the morphology of crystallinity of hydroxyapaptite nanoparticles, Journal of the European Ceramic Society, 23(10) (2002) 1697-1704

[81] Ines S. Neira, Yury V. Kolen'ko, Oleg I, Lebedev, Gustaaf Van Tendeloo, Himadri S. Gupta, Francisco Guitian, Masahiro Yoshimura, An Effective Morphology Control of Hydroxyapatite Crystals via Hydrothermal Synthesis, Crystal Growth and Design, 9(1) (2008) 466-474

[82] Peipei Wang, Caihong Li, Haiyan Gong, Xuerong Jiang, Hongqiang Wang, Kaixing Li, Effects of synthesis conditions on the morphology of hydroxyapatite nanoparticles produced by wet chemical process, Powder Technology, 203(2) (2010) 315-321

[83] Xinxin Zhao, S. Ng, B.C. Heng, J. Guo, L. Ma, T.T. Tan, K.W. Ng, S.C. Loo, Cytotoxicity of hydroxyapatite nanoparticles is shape and cell dependent, Archives of Toxicology, 87(6) 1037-1052 (2012) 1037-1052

[84] Huiron Le, Kiriuthika Natesan, Sundaram Pranti-Haran, Mechanical property and biocompatibility of co-precipitated nano hydroxyapatite-gelatine composites, Journal of Advanced Ceramics, 4(3) (2015) 237-243

[85] K.P. Sanosh, Min-Cheol Chu, A. Balakrishnan, Yong-Jin Lee, T.N. Kim, Seong-Jai Cho, Synthesis of nano hydroxyapatite powder that simulate teeth particle morphology and composition, Current Applied Physics, 9(6) (2009) 1459-1462

[86] Image of a Boeing 747, http://www.travelandleisure.com/airlines-airports/united-airlines/united-airlines-airplane-parts-auction

[87] Boeing 747 model kit, http://mfpilot.com/ebaypics/Hasegawa10118B747_1wm.jpg

[88] Injection molding process, https://en.wikipedia.org/wiki/Injection_moulding#/media/File:Injection_molding_diagram.svg

[89] Yigui Li, Sasaki Minoru, HaneLazuhiro, Micro-optical components based on silicon mold technology, Optics and Lasers in Engineering, 41(3) (2003) 545-552

[90] H. Oda, P. Wood, H. Ogiya, S. Miyoshi, O. Tsuji, Optimizing the SiC Plasma Etching Process for Manufacturing Power Devices, CS MANTECH Conference, (2015)

[91] Tatsuya Enomoto. Masahiko Denda, Akihiko Yasuoka, Hidefumi Nakata, Loading Effect and Temperature Dependence of Etch Rate in CF□ Plasma, Japanese Journal of Applied Physics, 18(1) (1979) 155-163

[92] G. Muralithran, S. Ramesh, The effects of sintering temperature on the properties of hydryoxyapatite, Ceramics International, 26(2) (1999) 221-230

[93] S. Ramesh, C.Y. Tan, R. Tolouei, M. Amiriyan, J. Purbolaksono, I. Sopyan, W.D. Teng, Sintering behavior of hydroxyapatite prepared from different routes, Materials and Design, 34 (2011) 148-154

[94] S. Ramesh, K.L. Aw, R. Tolouei, M. Amiriyan, C.Y. Tan, M. Hamdi, J. Purbolaksono, M.A. Hassan, W.D. Teng, Sintering properties of hydroxyapatite powders prepared using different methods, Ceramics International, 39(1) (2012) 111-119

[95] H. Oda, P. Wood, H. Ogiya, S. Miyoshi, O. Tsuji, Optimizing the SiC Plasma Etching Process for Manufacturing Power Devices, CS MANTECH Conference, (2015)

[96] Tatsuya Enomoto, Masahiko Denda, Akihiko Yasuoka, Hidefumi Nakata, Loading Effect and Temperature Dependence of Etch Rate in CF□ Plasma, Japanese Journal of Applied Physics, 18(1) (1979) 155-163

[97] Michael B. Frank, Steven E. Naleway, Tsuk Haroush, Chin-Hung Liu, Sze Hei Siu, Jerry Ng, Ivan Torres, Ali Ismail, Keyur Karandikar, Michael M. Porter, Olivia A. Graeve, Joanna McKittrick, Stiff, porous scaffolds from magnetized alumina particles aligned by magnetic freeze casting, Materials Science and Engineering C, 77 (2017) 484-492

[98] Michael B. Frank, Sze Hei Siu, Keyur Karandikar, Chin-Hung Liu, Steven E. Naleway, Michael M. Porter, Olivia A. Graeve, Joanna McKittrick, Synergistic structures form magnetic freeze casting with surface magnetized alumina particles and platelets, Journal of the Mechanical Behavior of Biomedical Materials, 76 (2017) 153-163

[99] Xingguo Cheng, Liisa Kuhn, Chemotherapy drug delivery from calcium phosphate nanoparticles, International Journal of Nanomedicine, 2(4) (2007) 667-674

[100] Freudig Barbara, Hogekamp Stefan, Schubert Helmar, Dispersion of powders in liquids in a stirred vessel, Chemical Engineering and Processing, 38(4-6) (1999) 525-532

[101] N. Thangamani, K. Chinnakali, F.D. Gnanam, The effect of powder processing on the desification, microstructure and mechanical properties of hydroxyapatite, Ceramics International. 28 (2002) 355-362.

[102] O. Prokopiev, I. Sevostianov, Dependence of the mechanical properties of sintered hydroxyapatite on the sintering temperature, Materials Science and Engineering A. 431 (2006) 218-227.

[103] G. Georgiou, J.C. Knowles, J.E. Barralet, Dynamic shrinkage behavior of hydroxyapatite and glass-reinforced hydroxyapatites, Journal of Materials Science, 39 (2004) 2205-2208.

[104] M. Muller, W. Bauer, H. J. Ritzhaupt-Kleissl, Low Pressure Injection Molding of Ceramic Micro Devices Using Sub-Micron and Nano Scaled Powders, (2008)

[105] C. Moseke, U. Gbureck, Tetracalcium phosphate: Synthesis, properties and biomedical uses, Acta Biomaterialia, 6(10) (2010) 3815-3823

[106] Jonas Grossenbacher, Maurizio R. Gullo, Raphael Grandjean, Thomas Kiefer, Jurgen Brugger, Sub micrometer ceramic structures fabricated by molding a polymer-derived ceramic, Microelectrical Engineering, 97 (2012) 272-275.